Research Square

Preprints are preliminary reports that have not undergone peer review.
They should not be considered conclusive, used to inform clinical practice,
or referenced by the media as validated information.

PfRab5a defines a divergent trafficking pathway required for apical organelle biogenesis in Plasmodium falciparum

Tim Gilberger

tim.gilberger@bnitm.de

Bernhard Nocht Institute for Tropical Medicine https://orcid.org/0000-0002-7965-8272

Guilherme Farias

Bernhard Nocht Institute for Tropical Medicine

Leah Zink

Bernhard Nocht Institute for Tropical Medicine

Thilo Page

Bernhard Nocht Institute for Tropical Medicine

Nick Piwon

Bernhard Nocht Institute for Tropical Medicine https://orcid.org/0009-0004-7447-0125

Joëlle Mesén-Ramírez

Bernhard Nocht Institute for Tropical Medicine https://orcid.org/0000-0001-7842-5867

Yangyang Guo

Bernhard Nocht Institute for Tropical Medicine

Christian Löw

European Molecular Biology Laboratory (EMBL) Hamburg https://orcid.org/0000-0003-0764-7483

Danny Wilson

University of Adelaide https://orcid.org/0000-0002-5073-1405

Joachim Matz

Bernhard Nocht Institute for Tropical Medicine https://orcid.org/0000-0002-0575-0412

Tobias Spielmann

https://orcid.org/0000-0002-3968-4601

José Cubillán-Marín

Bernhard Nocht Institute for Tropical Medicine

Article

Keywords:

Posted Date: August 20th, 2026

DOI: https://doi.org/10.21203/rs.3.rs-10653303/v1

License: This work is licensed under a Creative Commons Attribution 4.0 International License.
Read Full License

Additional Declarations: There is **NO** Competing Interest.

PfRab5a defines a divergent trafficking pathway required for apical organelle biogenesis in *Plasmodium falciparum*

Guilherme B. Farias[1,2,3]; Leah Zink[1,2,3]; Thilo N. Page[1,2,3]; Nick Piwon[1,2,3]; Joëlle Paolo Mesén-Ramírez[1,2,3]; Yangyang Guo[2]; Christian Löw[1,2,4]; Danny W. Wilson[1,2,5,6]; Joachim M. Matz[2]; Tobias Spielmann[2]; José Cubillán-Marín[1,2,3]; Tim-Wolf Gilberger[1,2,3*]

[1]Centre for Structural Systems Biology, Hamburg, Germany; [2]Bernhard Nocht Institute for Tropical Medicine, Hamburg, Germany; [3]University of Hamburg, Department of Biology, Hamburg, Germany; [4]European Molecular Biology Laboratory, Hamburg Unit, Hamburg, Germany; [5]Research Centre for Infectious Diseases, Adelaide University, Adelaide, Australia, [6]Institute for Photonics and Advanced Sensing, Adelaide University, Adelaide, Australia.

*Corresponding Author: tim.gilberger@bnitm.de

Abstract

During intraerythrocytic schizogony, malaria parasites assemble the apical secretory organelles micronemes and rhoptries *de novo*, which are required for host cell invasion. These apical organelles are thought to arise from post-Golgi vesicles. However, how the parasite's endolysosomal system regulates their biogenesis remains unclear. Here, we show that the small GTPase PfRab5a, a central regulator of early endocytic pathways in other eukaryotes, has been repurposed to control apical organelle biogenesis in *Plasmodium falciparum*. PfRab5a defines a previously uncharacterized compartment that connects the secretory pathway to micronemes and rhoptries. Conditional inactivation of PfRab5a disrupts trafficking to and formation of apical organelles, resulting in defective host cell invasion. Proximity-dependent biotinylation identified vesicle tethering and membrane fusion factors and Rab regulators that cooperate in this unique PfRab5a pathway. Together, our findings reveal how a canonical endocytic regulator has been repurposed within a highly divergent endolysosomal system to build invasion organelles essential for parasite proliferation.

Introduction

The apicomplexan parasite *Plasmodium falciparum* causes the majority of severe malaria. Despite several advances in pharmacology and vaccine development, malaria remains a heavy economic and disease burden for endemic countries, with over half a million deaths reported annually, the majority of whom children[1]. Understanding parasite biology is crucial to guide future drug and vaccine programs. *Plasmodium* spp. have a complex life cycle that spans different tissues in both the human and mosquito hosts, with the intraerythrocytic development cycle (IDC) being responsible for clinical malaria symptoms. During the IDC, parasites replicate within red blood cells (RBCs) via schizogony, generating daughter merozoites equipped with a unique repertoire of apical secretory organelles – the rhoptries and micronemes – essential for RBC invasion (Fig. 1a). The mechanisms underlying their biogenesis remains poorly understood, but are thought to rely on unconventional and highly divergent trafficking pathways[2].

The Rab family of small GTPases are major regulators of membrane trafficking pathways in eukaryotes[2]. Rab proteins associate with intracellular membranes and determine the identity of target organelles and allow specific cargo delivery by recruiting key vesicle trafficking factors[3]. They act as molecular switches that cycle between an active GTP-bound membrane-associated state and an inactive GDP-bound cytosolic state[4]. One of the best-characterised examples of Rab-dependent processes is the endosome maturation, which is coordinated by the sequential activity of Rab5 and Rab7[2]. Early endosomes are decorated with Rab5 and, while maturing to late endosomes and lysosomes, Rab5 is progressively replaced by Rab7[2]. This process is orchestrated by recruitment of specific factors, such as vesicle tethering complexes. For instance, Rab5 first promotes the recruitment of the class C core vacuole/endosome tethering (CORVET) complex in early endosomes, whereas Rab7 recruits the homotypic fusion and vacuole protein sorting (HOPS) complex in mature endosomes, leading to coordinated membrane fusion mediated by soluble N-ethylmaleimide-sensitive factor attachment protein receptor (SNARE) proteins[5,6].

Endosomal maturation through Rab conversion is conserved from yeast to humans, although variations to this mechanism exist in plants[7–9]. However, certain organisms such as apicomplexan parasites possess a highly divergent endolysosomal system, in which several canonical endosomal factors have been repurposed for the formation of specialised invasion organelles[10–12]. This raises the question of whether and which Rab GTPases associate with these unconventional compartments and contribute to the biogenesis of invasion organelles in apicomplexan parasites.

While these pathways remain poorly defined in *Plasmodium* parasites, studies in the related apicomplexan parasite *Toxoplasma gondii* have provided important insights into the vesicle trafficking pathways behind the biogenesis of apical organelles[11]. Dominant-negative overexpression of the Rab5 paralogs TgRab5A and TgRab5C, but not TgRab5B, disrupts cargo transport to apical secretory organelles[13]. These paralogs localise to the endosome-like compartments (ELCs), suggesting functional specialisation within the Rab5 family[13,14]. Recent studies in *P. falciparum* have

implicated other components of trafficking pathways, including the cargo receptor PfSortilin[15], the HOPS and CORVET tethering complexes[16], and the post-Golgi clathrin adaptor protein (AP) complex PfAP-1[17] in the formation of apical organelles. Among Rab GTPases, PfRab5a – but not its endocytosis-related paralog PfRab5b – has been reported to be essential during late schizogony of *P. falciparum*[18,19], but its function has yet to be defined. Based on the repurposing of other common endosomal factors and its function in late schizogony, we hypothesised that PfRab5a may regulate the trafficking from the trans-Golgi to the apical organelles.

In this study, we therefore investigated the function of PfRab5a in *P. falciparum* parasites. Using rapid conditional inactivation via knock-sideways (KS)[19–21], we show that PfRab5a is indispensable for assembly of micronemes and rhoptries, and its loss results in non-invasive merozoites. We also demonstrate that PfRab5a localises to an uncharacterised compartment distinct from Golgi and PfRab7 compartments. Proximity-dependent biotin identification (BioID) identified the guanine nucleotide exchange factor (GEF) of PfRab5a, the vacuolar protein sorting 9 (PfVPS9), whose inactivation impaired apical organelle biogenesis by altering the steady-state localization of PfRab5a. BioID also identified canonical vesicle tethering and fusion factors, such as the missing subunit for the CORVET complex, PfVPS8. Finally, we also present here several effectors, such as the uncharacterized protein PF3D7_0929700, whose inactivation affected rhoptry biogenesis, therefore implicating it in the PfRab5a trafficking pathway. Collectively, these findings reveal divergent features within the endosomal system of *P. falciparum* and provide insight into how canonical trafficking machinery was repurposed to generate invasion organelles.

Results

PfRab5a defines an uncharacterized post-Golgi compartment

To study PfRab5a (PF3D7_0211200) in *P. falciparum,* we utilized the previously generated N-terminally tagged GFP-2xFKBP-PfRab5a line (PfRab5a^{endo})[19]. Consistent with previous work[18,19], PfRab5a^{endo} localized in foci in the proximity to the parasite nuclei (Fig. 1b). A single focus was observed in trophozoites, with the number increasing as parasites progressed into multinucleated schizonts (Fig. 1b). At the end of the cycle, segmented schizonts presented a single focus per daughter merozoite (Fig. 1b). The localization of the PfRab5a compartment appears to be associated with the microtubule organizing center (Supplementary Fig. 2a), mimicking the replication of other vesicle trafficking compartments during *P. falciparum* schizogony[22]. To characterize this compartment, PfRab5a^{endo} was colocalized with three episomally expressed compartment specific markers: PfGRASP (cis-Golgi)[23], PfRab6 (trans-Golgi)[24] and PfRab7 (PfRab7 compartment)[25], each fused to mScarlet (mSc). All three markers were found in close proximity, but did not co-localize with PfRab5a^{endo} (Fig. 1c,d). Despite the apparent proximity to mSc-PfRab6 and mSc-PfRab7, further analysis using super-resolution by optical reassignment (SoRa) spinning disk confocal microscopy revealed a clear separation between the PfRab5a-positive compartment and the trans-Golgi and PfRab7 compartments (Fig. 1e,f).

Given that PfRab5a^{endo} appeared to reside in an uncharacterized compartment at the post-Golgi, the integrity of this compartment was assessed using Brefeldin A (BFA), a fungal toxin that induces redistribution of the Golgi proteins into the endoplasmic reticulum (ER)[26]. After BFA treatment, PfRab5a^{endo} remained associated with this compartment, although reduced, consistent with the phenotype observed for PfRab7 (Supplementary Fig. 2b)[25]. Altogether, these findings indicate that PfRab5a^{endo} localizes in a post-Golgi compartment that is spatially distinct from PfRab7 compartments. This segregation resembles the distribution of Rab5 and Rab7 in canonical eukaryotic endosomal systems[3]. However, we cannot exclude that PfRab5a and PfRab7 occupy distinct subdomains of the same organelle, as described for the ELCs of *T. gondii,* where both GTPases reside in spatially separated sub-compartments[13].

Figure 1

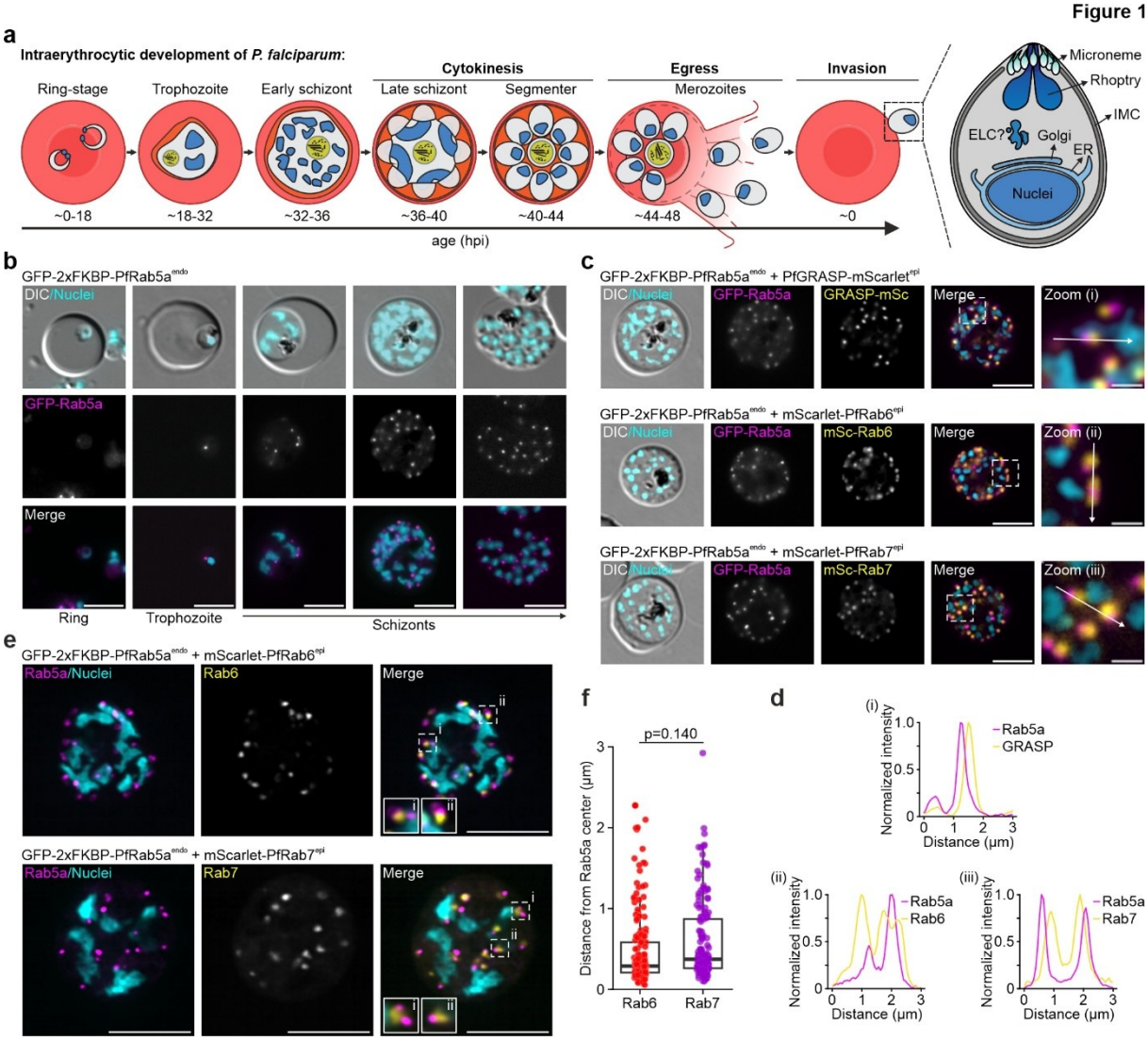


Figure 1. PfRab5a defines an uncharacterized post-Golgi compartment. a, Schematic representation of the intraerythrocytic development cycle (IDC) of *P. falciparum*, highlighting the cellular organization of the merozoite. ER, endoplasmic reticulum; ELC, endosome-like compartment; IMC, inner membrane complex. **b,** Live-cell fluorescence microscopy of PfRab5a^{endo} parasites throughout the IDC. **c,** PfRab5a^{endo} schizonts expressing episomal markers fused to mScarlet: PfGRASP-mSc (cis-Golgi), mSc-PfRab6 (trans-Golgi) and mSc-PfRab7 (PfRab7 compartments). **d,** Normalized fluorescence intensity plot of GFP (magenta) and mScarlet (yellow) signals from (**c**, i-iii). **e,** Live SoRa spinning disk confocal microscopy of PfRab5a^{endo} schizonts at 36-40 hpi expressing mSc-PfRab6 or mSc-PfRab7. **f,** Distance between the center of PfRab5a^{endo} foci and the center of the mSc-PfRab6 or mSc-PfRab7 foci. Data from n=10 schizonts per line (n=178 PfRab6^{epi} and n=149 PfRab7^{epi} focus measurements). Mean with SD; p-value, unpaired t-test. SoRa, Super-resolution by optical reassignment; DIC, differential interference contrast; Nuclei, Hoechst 33342; GFP, green fluorescence protein; mSc, mScarlet; Merge, overlay of magenta and cyan or magenta, yellow and cyan channels. Scale bars, 1 µm in (**c**, enlargements) and 5 µm in (**b**, **c**, **e**, whole cell).

PfRab5a is essential for invasion

To investigate the function of PfRab5a^{endo}, we conditionally inactivated this GTPase using the knock-sideways (KS) system[19]. This strategy allows a rapid mislocalization of the protein of interest to the nucleus using a nuclear mislocalizer (NLS), through rapalog-induced FKBP-FRB dimerization (Fig. 2a). PfRab5a-KS was induced in 0-4 hpi rings (early inactivation, Rapalog$_{0h}$) and 36-40 hpi schizonts (late inactivation, Rapalog$_{36h}$). Upon rapalog addition, PfRab5a^{endo} was successfully mislocalized to the nucleus (Supplementary Fig. 2c). Both inactivations resulted in a complete block in replication, confirming that PfRab5a is essential for parasite survival (Fig. 2b)[19].

To further characterize the KS phenotype, parasites were examined at different timepoints by Giemsa smears. Early inactivation exhibited arrested schizogony, resulting in aberrant parasites with ~5 nuclei (Fig. 2c and Supplementary Fig. 2d). Some of these parasites also presented a large vacuole-like structure from early schizonts onwards. Furthermore, no merozoites or new rings were observed, as previously reported[19]. In contrast, late inactivation did not affect schizogony as KS parasites displayed a number of nuclei similar to controls (Fig. 2c and Supplementary Fig. 2d). In these parasites, segmentation appeared normal, with individual merozoites visible. Despite a lack of clear morphological alterations during merozoite development, few rings (~4%) were observed during the expected transition to the next cycle, indicating that merozoite egress and/or invasion were severely impaired by PfRab5a loss. To corroborate this, schizont rupture (egress) and ring formation (invasion) were assessed. Late inactivation of PfRab5a resulted in a significant defect in merozoite invasion of RBCs, but not in parasite egress (Fig. 2d,e), indicating that PfRab5a is required for invasion.

As segmented schizonts were observed during late inactivation of PfRab5a (Fig. 2c), we investigated whether the integrity of the inner membrane complex (IMC), a double membrane organelle localized beneath the parasite plasma membrane (PPM)[27], was affected. To this end, the IMC marker PfIMC1c fused to mCherry (PfIMC1-mCh) was episomally co-expressed in PfRab5a^{endo} parasites. Late inactivation of PfRab5a did not affect the IMC integrity when compared to controls, although ~13% of parasites showed aberrant IMC localization (Supplementary Fig. 3a). Together, these results suggest that the PfRab5a trafficking pathway is critical for invasion, but loss of PfRab5a function is dispensable for formation of whole merozoites.

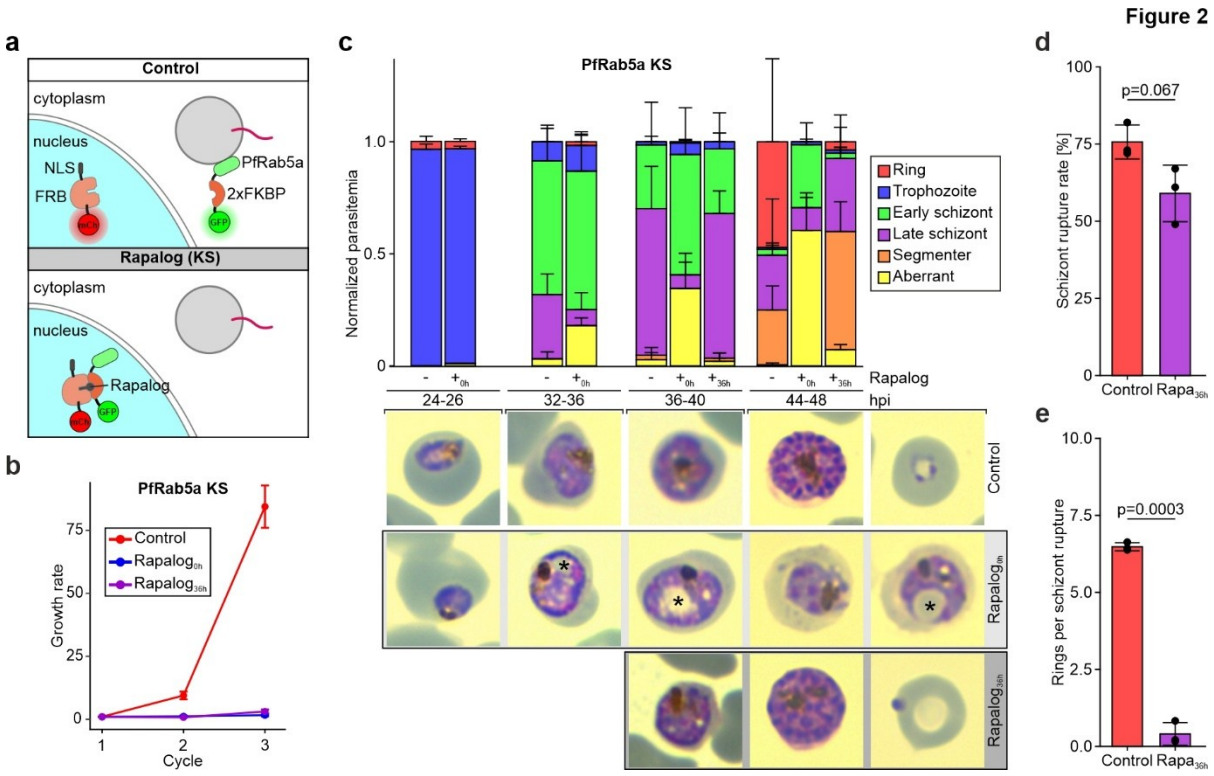


Figure 2. Conditional inactivation of PfRab5a leads to a defect in merozoite invasion. a, Schematic representation of the knock-sideways (KS) strategy, under normal conditions without rapalog (Control) and upon rapalog-induced mislocalization of PfRab5a to the nucleus (Rapalog). **b,** Growth curve of PfRab5a^{endo} parasites co-expressing the nuclear mislocalizer (NLS-FRB-mCherry) in controls and after early (0-4 hpi rings, Rapalog$_{0h}$) and late (36-40 hpi schizonts, Rapalog$_{36h}$) KS induction. Growth rate was normalized to initial parasitemia and measured over three cycles by flow cytometry (n=3 independent replicates per condition). **c,** Blood-stage parasite quantification of Giemsa smears at specified timepoints under normal condition (Control) and after early and late KS (Rapalog) induction. Bottom panel shows representative images of Giemsa smears at the different timepoints. Light grey box, Rapalog$_{0h}$; Dark grey box, Rabalog$_{36h}$. Asterisks (*) indicate abnormally large vacuolar structures. **d and e,** Parasite egress and invasion capability measured by schizont rupture rate (**d**) and rings per schizont rupture (**e**), respectively, before compound 2 (C2) removal (44-48 hpi) and subsequent parasite egress and invasion allowed to proceed for 8 hours. Parasites were grown in normal conditions and after late KS induction (Rapa$_{36h}$); parasitemia was measured by flow cytometry. Mean with SD; p-value, unpaired t-test.

Trafficking and processing of the microneme protein PfAMA1 depends on PfRab5a

Given that PfRab5a inactivation abrogates erythrocyte invasion, we questioned whether vesicle trafficking to micronemes was affected. To address this, the microneme marker apical membrane antigen 1 (PfAMA1) fused to mCherry (PfAMA1-mCh) was episomally co-expressed in PfRab5a^{endo} parasites. In addition, PfRab5a^{endo} was either inactivated (Rapalog$_{36h}$) or not (Control), and assessed at 44-48hpi in the presence of the cGMP-dependent kinase inhibitor Compound 2 (C2), which allows full schizont maturation without egress[28]. In control parasites, PfAMA1-mCh displayed the typical apical localization (Fig. 3a,b). In contrast, KS parasites exhibited defective localization, ranging from partial loss of apical localization with diffuse cytosolic signal to aberrant mistargeting of PfAMA1-mCh to the parasite periphery (Fig. 3a,b).

During parasite egress and immediately before invasion, PfAMA1 is proteolytically cleaved at two key steps, first inside the micronemes by Plasmepsin X (PfPMX) and then after translocation to the PPM by Subtisilin-2 (PfSUB2)[29] (Fig. 3c). To determine whether PfRab5a inactivation affected PfAMA1-mCh processing and secretion, KS and control parasites were allowed to mature in the presence of C2. Following schizont maturation, C2 was removed and parasites were incubated with the cysteine protease inhibitor E64, which allows microneme discharge and lysis of the parasitophorous vacuolar membrane (PVM) while preventing rupture of the RBC membrane[30]. This enabled the analysis of the microneme-contained PfAMA1-mCh in pre-egress schizonts (+C2) and secreted PfAMA1-mCh retained within infected RBCs after egress (+E64). KS and control schizonts from both conditions were collected and analyzed by western blot for processing of PfAMA1-mCh (Fig. 3d). Quantification of band signals revealed that KS parasites accumulated the unprocessed 110 kDa form of PfAMA1-mCh (PfAMA1$_{83}$-mCh, in pre- and post-egress) compared to controls (Fig. 3d,e), suggesting that PfAMA1-mCh mistargeting caused by PfRab5a inactivation also affected the proper maturation of this microneme protein.

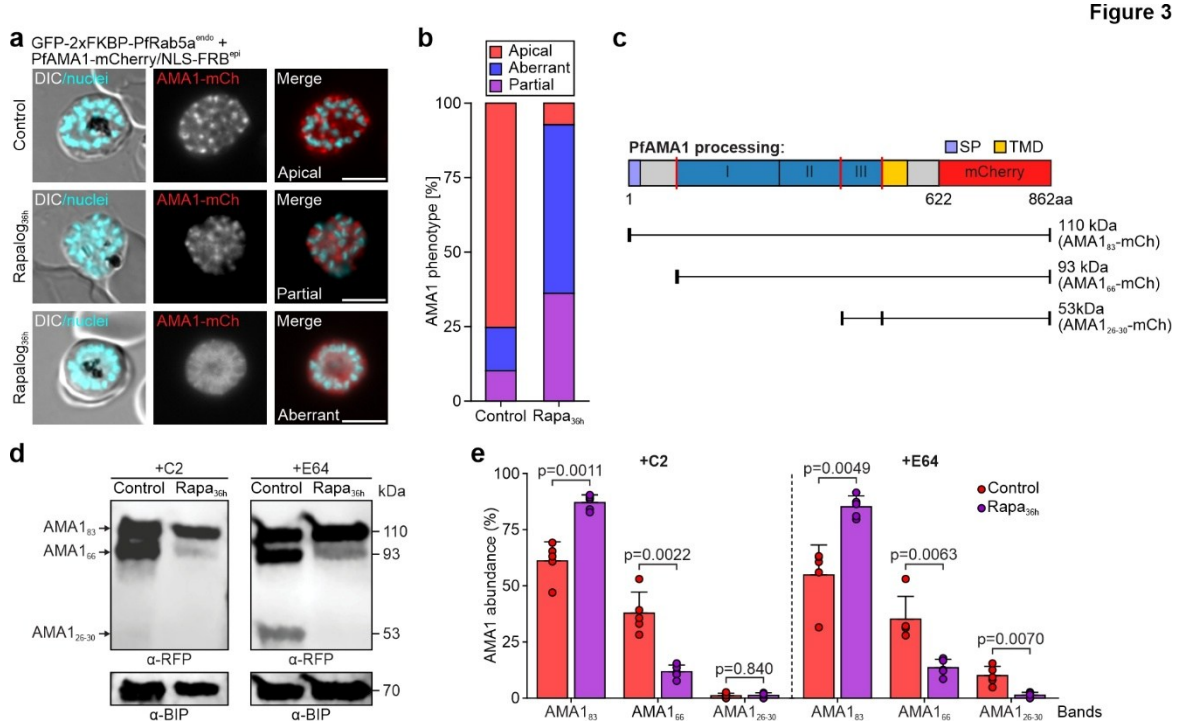


Figure 3. PfRab5a loss alters PfAMA1 trafficking and maturation. a, Live-cell fluorescence microscopy of control and KS ($Rapalog_{36h}$) $PfRab5a^{endo}$ schizonts episomally expressing PfAMA1-mCh. C2 was added to prevent egress and parasites were imaged at 44-48 hpi. Control parasites showed apical distribution of PfAMA1 whereas in the majority of KS parasites, PfAMA1 signal had either partial mislocalization with foci and diffuse pattern, or aberrant localization defined by peripheric localization. DIC, Differential interference contrast; Nuclei, Hoechst 33342; Merge, overlay of red and cyan channels. Scale bars, 5 μm. **b,** Quantification of PfAMA1-mCh phenotype in control and KS parasites from (**a**), n=60 parasites per condition from 2 independent experiments. **c,** Schematic representation of PfAMA1-mCh, illustrating the AMA1 domains (I to III) and the proteolytic cleavage sites (red lines) from the unprocessed 110 kDa form ($PfAMA1_{83}$-mCh) to the 93 kDa ($PfAMA1_{66}$-mCh) and 53 kDa ($PfAMA1_{26\text{-}30}$-mCh) forms. SP, signal peptide; TMD, trans-membrane domain; aa, amino acids. **d,** Control and KS parasites were arrested with C2 until the 48-52 hpi timepoint to prevent egress (+C2), schizonts were isolated and then treated with E64 to allow merozoite egress from the PVM without RBC membrane rupture (+E64). Parasites were isolated from both conditions (+C2 and +E64) and analyzed by western blot. A representative replicate from 5 independent experiments is shown. α-RFP, anti-red fluorescent protein (RFP) antibody; α-BIP (loading control), anti-binding immunoglobulin protein (BIP) antibody. **e,** Comparison of total PfAMA1-mCh protein abundance across 5 independent biological replicates measured by signal intensity from (**d**). Mean with SD; p-values, unpaired t-test.

PfRab5a is required for rhoptry trafficking and biogenesis

Next, we examined the rhoptries, a pair of club-shaped organelles essential – like the micronemes – for invasion[31]. To assess their integrity after PfRab5a inactivation, we applied ultrastructural expansion microscopy (U-ExM) and staining with N-hydroxysuccinimide (NHS) ester, a fluorescent dye that labels protein-dense structures such as rhoptries and the centriolar plaque (CP)[22]. Upon late inactivation of PfRab5a, KS parasites displayed malformed rhoptries compared to controls (Fig. 4a,b). This defect could also be visualized in living parasites with the rhoptry bulb marker Armadillo repeat-only (PfARO) fused to mCherry (PfARO-mCh) (Supplementary Fig. 3b)[32,33]. Quantitative volume analysis of the rhoptries based on either NHS and PfARO-mCh signals confirmed a significant volume reduction in KS parasites (Fig. 4c and Supplementary Fig. 3c), confirming a clear defect in rhoptry biogenesis.

Since a reduction in rhoptry bulb volume was observed, we hypothesized that PfRab5a loss may impact rhoptry contents. To test this, we used PfRab5a^{endo} parasites episomally co-expressing rhoptry neck protein 12 (PfRON12) fused to mCherry (PfRON12-mCh), a luminal rhoptry neck protein[34,35]. In addition, specific antibodies against the rhoptry-associated protein 1 (PfRAP1)[36], which resides in the lumen of the rhoptry bulb, was assessed in expanded samples. Whereas PfRON12-mCh and PfRAP1 displayed an apical localization in control parasites, the cellular localization of both rhoptry markers was affected in KS parasites (Fig. 4d and Supplementary Fig. 3d). This altered distribution suggested that rhoptry protein processing, like microneme protein processing, might also be affected. During egress, PfRAP1 (84 kDa) is processed by Plasmepsin IX (PfPMIX) and Subtilisin-1 (PfSUB1) into a 67 kDa product in released merozoites[37] (Fig. 4e). Western blot analysis showed that KS parasites exhibited a significant accumulation of unprocessed PfRAP1 compared to controls, suggesting that PfRAP1 processing was impacted as observed for PfAMA1-mCh, although to a less pronounced extent (Fig. 4f,g). Collectively, these results indicate that the PfRab5a pathway is important for rhoptry formation and likely rhoptry protein function.

Figure 4

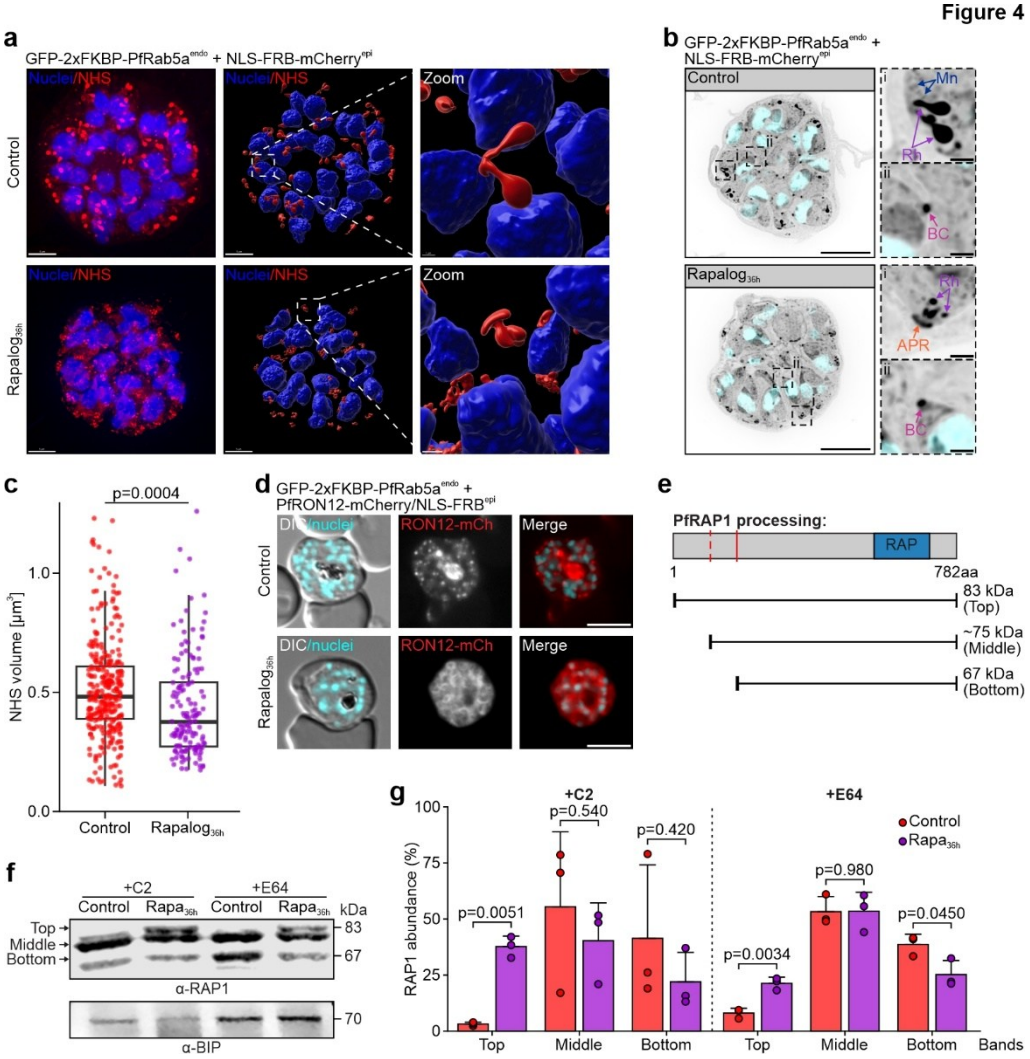


Figure 4. PfRab5a is required for rhoptry biogenesis. a, Ultra-structure expansion microscopy (U-ExM) of control and KS (Rapalog$_{36h}$) PfRab5a^{endo} parasites. C2 was added to prevent egress until 44-48 hpi. U-ExM samples were stained with NHS-ester for rhoptries (red) and Hoechst 33342 for nuclei (blue). Left and middle panels show maximum intensity projection and Imaris-generated 3D reconstructions, respectively. Boxed areas were enlarged (Zoom, 300%). **b,** U-ExM of control and KS (Rapalog$_{36h}$) schizonts arrested with C2 at 44-48 hpi and stained with NHS-ester (grayscale) and DAPI (cyan). Zoom panels highlight major structures stained with NHS: micronemes (Mn, blue arrow); rhoptries (Rh, purple arrow); apical polar ring (APR, orange arrow); and constricted basal complex (BC, pink arrow). U-ExM samples imaged with SoRa spinning disk confocal microscopy (z-step = 0.15 µm). SoRa, Super-resolution by optical reassignment. **c,** Quantification of rhoptry volume from (**a**), n=10 schizonts per condition from two independent experiments. **d,** Live-cell fluorescence microscopy of control and KS PfRab5a^{endo} schizonts co-expressing PfRON12-mCh (rhoptry neck). DIC, Differential interference contrast; Nuclei, Hoechst 33342; Merge, overlay of red and cyan channels. Scale bars, 1 µm in (**b**, enlargements) and 5 µm in (**a**, **b**, **d**, whole cell). **e,** Schematic representation of PfRAP1, illustrating the proteolytic processing of this rhoptry protein from the unprocessed 83 kDa form (Top) to the ~75 kDa (Middle) and 67 kDa (Bottom) forms. **f,** Control and KS parasites were arrested with C2 to prevent egress until 48-52 hpi (+C2). Schizonts were then isolated and kept instead on E64 to allow merozoite egress from the PVM without RBC membrane rupture (+E64). Parasites were isolated from both conditions

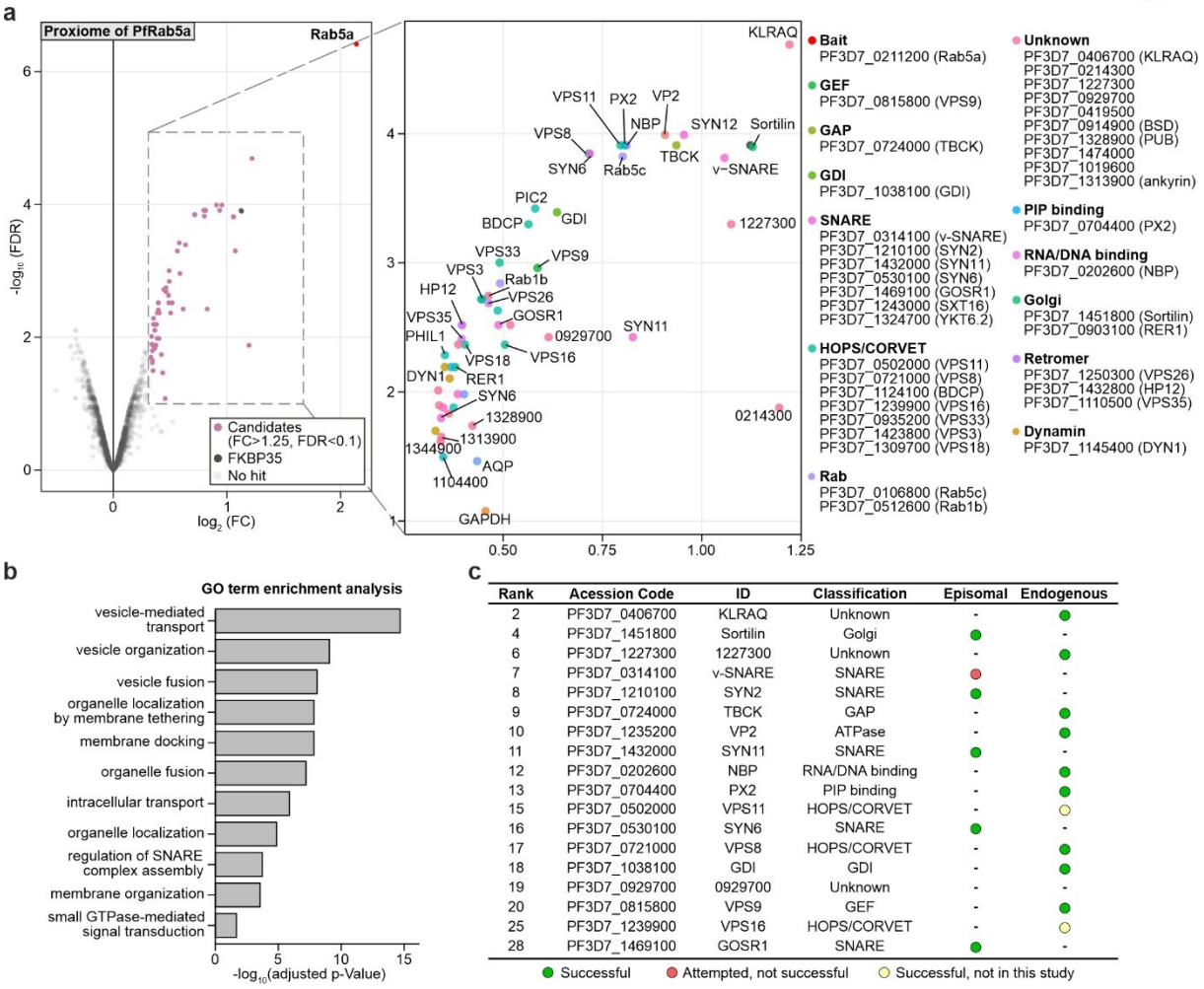
(+C2 and +E64) and analyzed by western blot. **g,** Percentage of total PfRAP1 abundance from (**f**). Mean with SD; p-values, unpaired t-test.

Proxiome of PfRab5a reveals an unconventional, yet conserved, vesicle trafficking machinery

To better define the PfRab5a-associated vesicle trafficking pathway, dimerization-induced quantitative proximity biotinylation (DIQ-BioID)[38] was used to identify the potential interacting partners of PfRab5a. In this system, the promiscuous biotin ligase miniTurbo is C-terminally tagged with FRB-mCherry (miniTurbo-FRB-mCherry) and expressed in PfRab5a^{endo} parasites. In the absence of rapalog (Control), the biotin ligase was detected in the parasite cytosol (Supplementary Fig. 4a,b). Upon addition of rapalog, miniTurbo is recruited to PfRab5a foci through FKBP-FRB dimerization (Supplementary Fig. 4a,b), enabling proximity-dependent biotinylation of PfRab5a-associated proteins. To minimize biotinylation background and capture stage-specific interactions in living parasites, 36-44 hpi schizonts were incubated with or without rapalog for 50 minutes, with a biotin pulse during the final 30 minutes of rapalog incubation. Efficient and rapalog-dependent biotinylation was confirmed by western blot (Supplementary Fig. 4c). Biotinylated proteins were subsequently identified by quantitative mass spectrometry analysis, normalized and compared to controls to define the PfRab5a proxiome (Fig. 5a and Supplementary Data 1).

The proxiome of PfRab5a identified 57 enriched proteins (fold change (FC)>1.25, false discovery rate (FDR)<0.1), including the bait itself, PfRab5a (Fig. 5a and Supplementary Data 1). Gene ontology (GO) analysis revealed strong enrichment for vesicle trafficking-related processes, including transport, tethering, and membrane fusion (Fig. 5b). For instance, one of the top enriched hits was PfSortilin (PF3D7_1451800), a canonical multiligand receptor involved in cargo sorting at the trans-Golgi[15,39]. Furthermore, a prominent group featured in the PfRab5a proxiome were SNARE proteins, which mediate membrane fusion[40]. Seven SNAREs were detected, with different levels of enrichment (Fig. 5a). Similarly, components of the tethering complexes HOPS and CORVET[16,41] and components of the retromer complex[25] including PfVPS26 (PF3D7_1220300) and PfVPS35 (PF3D7_1110500), as well as the putative GEF PfVPS9 (PF3D7_0815800) were identified. Interestingly, two additional small Rab GTPases were detected (Fig. 5a): the Rab5 paralog PfRab5c (PF3D7_0106800), and PfRab1b (PF3D7_0512600). Furthermore, proteins with unknown function and limited domain annotation such as PF3D7_0406700 (KLRAQ domain-containing protein), PF3D7_1227300 (unknown function), PF3D7_0202600 (nucleic acid binding protein, PfNBP), PF3D7_0704400 (PX domain-containing protein, PfPX2) and PF3D7_0929700 (unknown function) where among the top 20 proteins enriched in the PfRab5a proxiome that might represent potential effectors in vesicle transport (Fig. 5c).

Figure 5



Rank	Acession Code	ID	Classification	Episomal	Endogenous
2	PF3D7_0406700	KLRAQ	Unknown	-	●
4	PF3D7_1451800	Sortilin	Golgi	●	-
6	PF3D7_1227300	1227300	Unknown	-	●
7	PF3D7_0314100	v-SNARE	SNARE	●	-
8	PF3D7_1210100	SYN2	SNARE	●	-
9	PF3D7_0724000	TBCK	GAP	-	●
10	PF3D7_1235200	VP2	ATPase	-	●
11	PF3D7_1432000	SYN11	SNARE	●	-
12	PF3D7_0202600	NBP	RNA/DNA binding	-	●
13	PF3D7_0704400	PX2	PIP binding	-	●
15	PF3D7_0502000	VPS11	HOPS/CORVET	-	○
16	PF3D7_0530100	SYN6	SNARE	●	-
17	PF3D7_0721000	VPS8	HOPS/CORVET	-	●
18	PF3D7_1038100	GDI	GDI	-	●
19	PF3D7_0929700	0929700	Unknown	-	-
20	PF3D7_0815800	VPS9	GEF	-	●
25	PF3D7_1239900	VPS16	HOPS/CORVET	-	○
28	PF3D7_1469100	GOSR1	SNARE	●	-

● Successful ● Attempted, not successful ○ Successful, not in this study

Figure 5. The PfRab5a proxiome. a, Volcano plot showing the proteins enriched in the PfRab5a DiQ-BioID. Proteins were considered candidate interactors if fold-change (FC)>1.25 and false discovery rate (FDR)<0.1. Zoom inlet of candidates colored in general groups and named based on either gene name or main annotated domain. Each protein in the group is ordered based on its FC enrichment. **b,** Gene ontology (GO) term enrichment analysis of significant biological process terms for the enriched candidates identified in PfRab5a proxiome (Benjamini-Hochberg method adjusted p-value<0.05). **c,** Summary table showing the 18 candidates selected for validation, displaying if the candidate was investigated by episomal expression (Episomal) or by endogenous tagging (Endogenous). GEF, Guanine exchange factor; GAP, GTPase-activating protein; GDI, Guanosine nucleotide dissociation inhibitor; SNARE, Soluble NSF attachment protein receptor; HOPS, Homotypic fusion and vacuole protein sorting; CORVET, Class C core vacuole/endosome tethering; PIP, Phosphatidylinositol phosphate.

SNAREs and Sortilin localize in PfRab5a compartments

Within the group of selected proteins for further validation, we first started with a group of known cargo sorting and fusion proteins. Episomal co-expression of PfSortilin fused to mScarlet (PfSortilin-mSc) showed that this receptor colocalized with PfRab5a^{endo} (Supplementary Fig. 4d). Upon early inactivation of PfRab5a, PfSortilin-mSc localization was partially disrupted, exhibiting a dispersed dotted pattern (~88%) in the parasite cytosol (Supplementary Fig. 4d). The four most enriched SNAREs PfSYN2 (PF3D7_1210100), PfSYN11 (PF3D7_1432000), PfSYN6 (PF3D7_0530100) and PfGOSR1 (PF3D7_1469100) were N-terminally tagged with mScarlet (mSc-PfSYN2, mSc-PfSYN11, mSc-PfSYN6, mSc-PfGOSR1) and expressed in PfRab5a^{endo} parasites. mSc-PfSYN6 and mSc-PfSYN11 were found to colocalize with PfRab5a^{endo} (Supplementary Fig. 4e). These SNAREs also displayed additional localizations that did not correspond to PfRab5a^{endo}: mSc-PfSYN6 localized to the food vacuole (FV) membrane and mSc-PfSYN11 exhibited a vesicle-like pattern throughout the parasite cytosol (Supplementary Fig. 4e). In contrast, mSc-PfSYN2- and mSc-PfGOSR1-positive puncta were close to PfRab5a compartments, but did not overlap (Supplementary Fig. 4e). In our hands, the highly enriched Pfv-SNARE PF3D7_0314100 could not be expressed as a mScarlet fusion protein. Taken together, these findings indicate that PfSortilin and at least 2 SNAREs intersect at the PfRab5a compartments, consistent with their high-confidence enrichment in the BioID dataset.

One of the most enriched proteins not associated with vesicle trafficking roles was the V-type K^+-independent H^+-translocating inorganic pyrophosphatase (PfVP2, PF3D7_1235200). In order to investigate its function, a conditional knockout (cKO) line for PfVP2 fused with mCherry in its C-terminus (PfVP2-mCh^{endo}) was generated, with PfVP2-mCh^{endo} only expressed as cytosolic foci in late schizonts (Supplementary Fig. 4f). However, the PfVP2-mCh^{endo} cKO did not affect parasite proliferation (Supplementary Fig. 4g), as was previously reported[42]. The enrichment of PfVP2-mCh^{endo} in the PfRab5a proxiome suggests that this pyrophosphatase might reside in the PfRab5a compartment or its final destination depends on the PfRab5a trafficking pathway.

PfRab5a-BioID identifies an elusive PfVPS8 subunit of the CORVET complex

The HOPS and CORVET complexes are the major tethering factors involved in the fusion of endolysosomal compartments in eukaryotes[6]. Both complexes share a set of core subunits consisting of VPS11, VPS16, VPS18 and VPS33 (Fig. 6a), which we recently characterized in *P. falciparum*[16]. The PfRab5a BioID identified these HOPS/CORVET core subunits and the CORVET-specific subunit PfVPS3 (PF3D7_1423800) (Fig. 5a and 6b). We validated the core subunits PfVPS11 and PfVPS16 by co-localization with the episomal PfRab5a N-terminally fused to mScarlet (mSc-PfRab5a). PfVPS11^{endo} colocalized with mSc-PfRab5a in a subset of foci in schizont-stage parasites, whereas PfVPS16^{endo} exhibited almost complete colocalization with mSc-PfRab5a (Supplementary Fig. 5a).

Among the top 20 proteins enriched in the PfRab5a DiQ-BioID was the uncharacterized protein PF3D7_0721000, which was recently proposed as a putative PfVPS8, based on its identification in a PfVPS16 pulldown[41]. We used AlphaFold3[43] to predict the structure of PF3D7_0721000, and we then compared this model with the mammalian and yeast VPS8 proteins. This revealed that PF3D7_0721000 possesses conserved structural features of VPS8 proteins, particularly the N-terminal β-propeller. Structural alignment of the modelled PF3D7_0721000 β-propeller (498-1071 aa) with the N-terminal β-propellers of mouse (UniProt: Q0P5W1 95-515 aa), human (UniProt: Q8N3P4 95-513 aa) and yeast (UniProt: O13756 93-513 aa) VPS8 yielded Template Modelling scores (TM-score) of 0.53, 0.52 and 0.51, respectively (Fig. 6c,d and Supplementary Fig. 5b), supporting PF3D7_0721000 as a putative *Plasmodium* VPS8 homolog. Hereafter, we refer to PF3D7_0721000 as PfVPS8.

As we were unable to make a C-terminally tagged line, we generated an N-terminal-tagged PfVPS8^{endo} parasite line using CRISPR/Cas9 to validate this putative CORVET subunit. Parasites expressing mNeonGreen-3xHA-PfVPS8^{endo} showed expression of the fusion protein from trophozoites to merozoites with a punctate pattern (Fig. 6e), which colocalized with mSc-PfRab5a (Fig. 6f), indicating that this CORVET subunit resides in PfRab5a compartments.

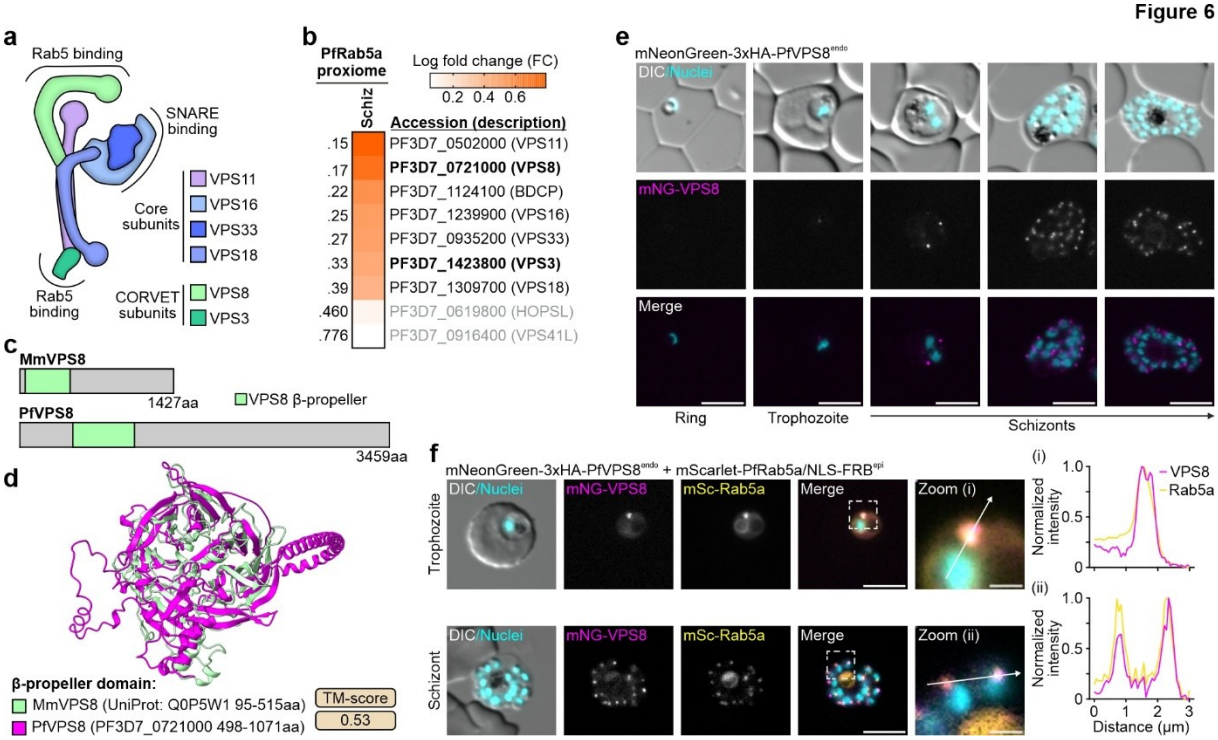


Figure 6. PfRab5a DiQ-BioID identified the missing CORVET-specific subunit PfVPS8. a, Schematic representation of the CORVET complex based on Cryo-EM structure from yeast[44]. Core subunits are shared with HOPS complex (blue-to-purple). The CORVET subunits VPS8 (light green) and VPS3 (dark green) interact with Rab5, whereas the Core subunits VPS16 light blue) and VPS33 (dark blue) possess a SNARE-binding module. **b,** Heatmap with the putative *P. falciparum* HOPS/CORVET subunits ordered by Log_2 fold change (FC) and corresponding rank in the PfRab5a proxiome (schizont stage). Putative PfRab5a-binding CORVET-specific subunits are in bold (PfVPS8 and PfVPS3) whereas the putative PfRab7-binding HOPS-specific subunits are in grey (HOPSL and VPS41L). Schiz, Schizont. **c,** Schematic representation of the *Mus musculus* and *P. falciparum* VPS8 proteins. **d,** Structure alignment of VPS8 β-propeller domains from *M. musculus* (UniProt: Q0P5W1 95-515 aa, green) and *P. falciparum* (PF3D7_0721000, 498-1071 aa, magenta) modelled using AlphaFold3[43]. Template modelling scores (TM-score) were calculated with FoldSeek[45]; TM-scores > 0.5 indicate high structural similarity between compared structures[46]. **e and f,** Live-cell fluorescence microscopy of mNeonGreen-3xHA-PfVPS8^{endo} parasites (PfVPS8^{endo}) throughout the cycle (**e**) or trophozoite and schizonts episomally expressing mSc-PfRab5a (**f**). Normalized fluorescence intensity plots of PfVPS8^{endo} and mSc-PfRab5a from (i and ii). DIC, Differential interference contrast; Nuclei, Hoechst 33342; Merge, overlay of magenta and cyan or magenta, yellow and cyan channels. Scale bars, 1 μm in (**f**, enlargements) and 5 μm in (**e**, **f**, whole cell).

PfVPS9 is an essential regulator of PfRab5a

VPS9 domain-containing proteins are canonical GEFs of the Rab5 family of proteins[47]. GEFs, in conjunction with GTPase-activating proteins (GAPs) and GDP dissociation inhibitor (GDI), tightly regulate the Rab cycle[48]. The potential homolog of VPS9 in the parasite proteome PfVPS9 (PF3D7_0815800) was identified in the PfRab5a BioID (Fig. 5a) – also within the top 20 enriched proteins. With 1833 aa, this protein (Fig. 7a) is more than three times the size of its yeast counterpart (UniProt: P54787 451 aa). Despite this, AlphaFold3 predictions support a direct interaction of PfVPS9 and PfRab5a (Fig. 7b and Supplementary Fig. 6a), with a relatively high interaction confidence score of 0.77 for the interface predicted Template Modeling (ipTM) and 0.61 for the interaction prediction Score from Aligned Errors (ipSAE) of the VPS9 domain with PfRab5a. Furthermore, this predicted interface is constituted by two conserved α-helices in the VPS9 domain that form a hydrophobic groove previously implicated in Rab5 interactions[47].

Next, we characterized this putative GEF in more detail. PfVPS9 was endogenously tagged with the 2xFKBP-GFP-2xFKBP tag, with an additional NLS-FRB cassete[16,19] that allows its co-expression with the nuclear mislocalizer (PfVPS9/NLS^{endo}). We first showed that PfVPS9 is expressed in trophozoites and schizonts exhibiting a PfRab5a-like punctate pattern (Supplementary Fig. 6b). Second, we co-expressed mSc-PfRab5a in these transgenic parasites revealing co-localization of both proteins (Fig. 7c). Importantly, upon mis-localization of PfVPS9 to the nucleus, the localization of mSc-PfRab5a was completely altered, displaying a diffuse cytosolic pattern (Fig. 7c), characteristic of the inactive GDP-bound state of Rab GTPases[49].

Subsequently, we analyzed the physiological consequences of PfVPS9 inactivation. By inducing the mislocalization of PfVPS9 in ring and schizont stages, we found that KS parasites displayed a pronounced growth defect compared to the control (Supplementary Fig. 6c,d). A more detailed analysis using stage quantification of Giemsa smears revealed that late inactivation of PfVPS9 led normal parasite development to segmented schizonts, but in the subsequent cycle no new rings were detected (Supplementary Fig. 6e). To confirm this, schizont rupture (egress) and ring formation (invasion) were examined in PfVPS9-KS. Similar to PfRab5a, late inactivation of PfVPS9 resulted in a significant reduction in invasion, but not in egress (Supplementary Fig. 6d). This resembles the PfRab5a phenotype and suggests a defect in apical organelle biogenesis and supports its role as a GEF for PfRab5a.

To investigate whether PfVPS9 inactivation affected apical organelle biogenesis, PfAMA1-mCh and PfARO-mCh were expressed in PfVPS9/NLS^{endo} parasites. In control parasites, PfAMA1-mCh was localized to the apical region (Fig. 7d). Upon PfVPS9 inactivation, PfAMA1-mCh apical localization was affected (Fig. 7d). Next, we investigated the impact of PfVPS9-KS on rhoptry integrity by spinning disk confocal microscopy. Control parasites showed the characteristic distribution of PfARO-mCh in rhoptry bulbs, while KS parasites exhibited smaller punctate PfARO-mCh signal (Fig. 7e). Taken together, these findings resemble the PfRab5a-KS phenotype and functionally link PfVPS9 with PfRab5a.

Beside PfVPS9, the PfRab5a proxiome also disclosed a putative GAP (TBC domain-containing kinase or TBCK, PF3D7_0724000)[50] as well as a putative GDI (PF3D7_1038100), both of which play a regulatory role in the Rab5 cycle in other eukaryotic systems[48]. By tagging both proteins using SLI system, we showed that the putative PfTBCK, which exhibits a punctate pattern in trophozoites and schizonts (Supplementary Fig. 6f), colocalized with mSc-PfRab5a (Supplementary Fig. 6h). Conditional knockdown (cKD) of PfTBCK-glmS^{endo} showed no significant difference in the fluorescence intensity compared to the control after three cycles (Supplementary Fig. 6g). The putative PfGDI displayed a cytosolic localization, with some foci observed in trophozoites and early schizonts (Supplementary Fig. 6i) that colocalized with mSc-PfRab5a (Supplementary Fig. 6k). This localization is consistent with GDI function, which binds to cytosolic GDP-bound Rabs[48,49,51]. However, conditional inactivation of this PfGDI did not affect parasite growth (Supplementary Fig. 6j).

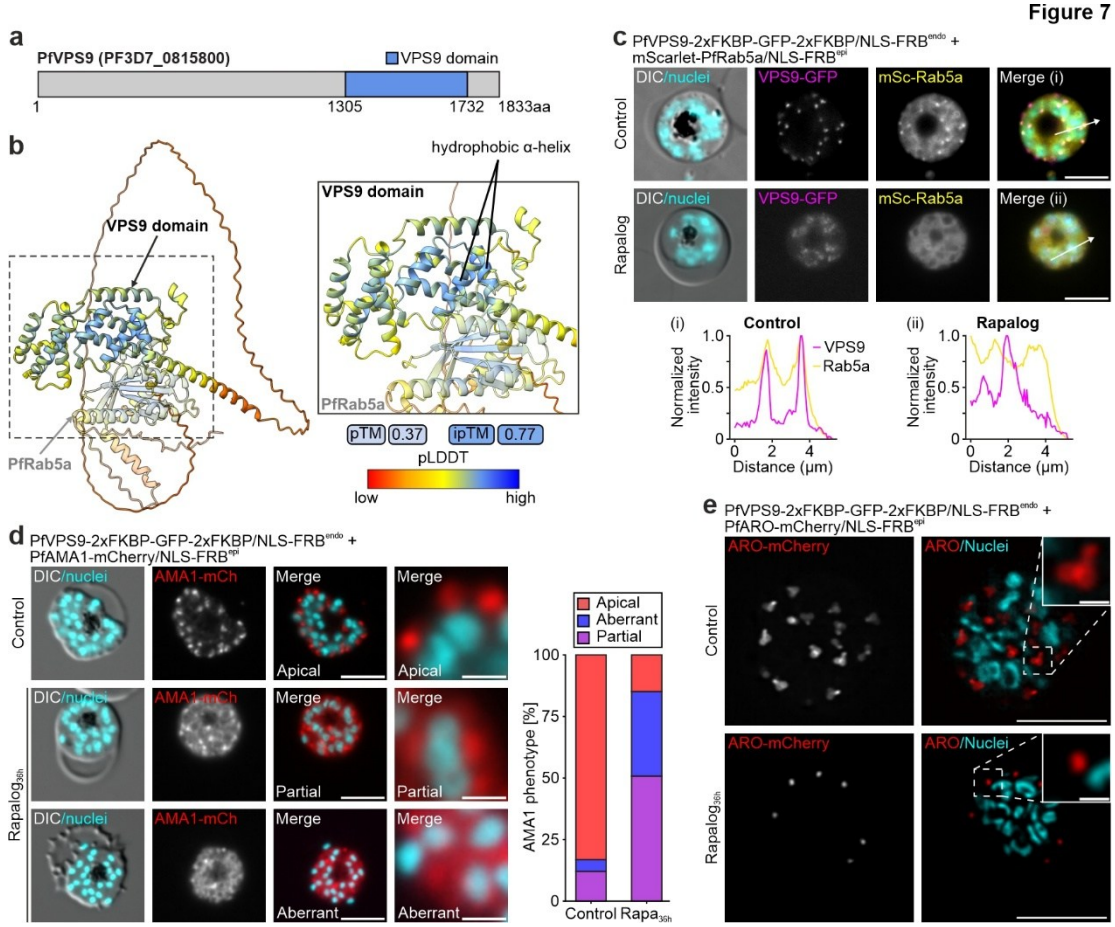


Figure 7. PfVPS9 is critical for PfRab5a function. a, Schematic representation of PfVPS9. **b,** Predicted interaction of VPS9 domain (1305-1732 aa) and PfRab5a using AlphaFold3[43]. Prediction shows residues with predicted Local Distance Difference Test (pLDDT) above 50 for the VPS9 domain and the whole PfRab5a (transparent). Zoom shows enlargement of the region delimited by dotted box, displaying the predicted interaction of PfRab5a with two hydrophobic α-helix of the VPS9 domain. pTM, predicted Template Modelling score; ipTM, interface predicted Template Modeling. **c,** Live-cell fluorescence microscopy of control and KS ($Rapalog_{36h}$) PfVPS9-2xFKBP-GFP-2xFKBP/NLS-FRB^{endo} ($PfVPS9/NLS^{endo}$) co-expressing mSc-PfRab5a. Normalized fluorescence intensity plots of PfVPS9 and mSc-PfRab5a from (i and ii). **d,** Control and KS ($Rapalog_{36h}$) $VPS9/NLS^{endo}$ parasites episomally co-expressing PfAMA1-mCh and imaged at 44-48 hpi. Control parasites showed normal apical PfAMA1-mCh signal distribution while in most KS parasites, PfAMA1-mCh signal had either partial mislocalization with foci and diffuse pattern, or aberrant localization. PfAMA1-mCh phenotype of n=25 parasites from three experiments. **e,** SoRa spinning disk confocal microscopy of control and KS ($Rapalog_{36h}$) $PfVPS9/NLS^{endo}$ parasites episomally co-expressing PfARO-mCh and imaged at 48-52 hpi. Compound 2 (C2) was added to prevent egress. Zoom shows enlargements of the region delimited by dotted box, displaying apical PfARO-mCh signal. SoRa, Super-resolution by optical re-assignment. DIC, Differential interference contrast; Nuclei, Hoechst 33342; Merge, overlay of magenta, yellow and cyan or red and cyan channels. Scale bars, 1 μm in (**d**, **e**, enlargements) and 5 μm in (**c**-**e**, whole cell).

Novel candidates associated with PfRab5a-dependent organelle biogenesis

Among the top 20 proteins enriched in the PfRab5a-BioID dataset were several proteins with unknown function or domains that may reside in the same intracellular compartment as PfRab5a (Supplementary Fig. 7a-e). We therefore selected five candidates for further characterization: PF3D7_0406700 (KLRAQ domain-containing protein, PfKLRAQ), PF3D7_1227300 (unknown function), PF3D7_0202600 (nucleic acid binding protein, PfNBP), PF3D7_0704400 (PX domain-containing protein 2, PfPX2) and PF3D7_0929700 (unknown function). A C-terminal 2xFKBP-GFP-2xFKBP tag was added to PfKLRAQ, PfNBP, PfPX2 and PF3D7_0929700 using the SLI system[19], whereas PF3D7_1227300, which could not be tagged via the SLI system in our hands, was generated by placing an N-terminal mNeonGreen-3xHA tag using CRISPR/Cas9[52]. All five proteins displayed a punctate distribution throughout the cytosol of trophozoites and schizonts (Supplementary Fig. 7a-e). Co-expression with mSc-PfRab5a showed that each candidate localized to PfRab5a compartments (Fig. 8a). However, conditional inactivation of SLI-generated candidates (PfKLRAQ, PfPX2 and PF3D7_0929700) did not alter PfRab5a localization (Supplementary Fig. 7f). Growth assays further showed that only PfKLRAQ^{endo}, PfPX2^{endo} and PF3D7_0929700^{endo} were required for parasite proliferation (Fig. 8b and Supplementary Fig. 7g). The lack of a growth phenotype in PfNBP-KS may be explained by its inefficient mislocalization to the parasite nucleus (Supplementary Fig. 7g).

We next sought to validate candidates using complementary approaches. Given that PfPX2 represented the only candidate with a PX domain that binds to phosphatidylinositol phosphate (PIP), having been reported to preferentially bind PI_3P, PI_5P and $PI_{(3,5)}P_2$[53], we tested whether it physically associates with PfRab5a. To this end, we generated a cell line expressing endogenously tagged PfPX2 fused to mScarlet (PX2^{endo}) in PfRab5a^{endo} parasites via SLI2[54]. Reciprocal pulldown using either PfRab5a^{endo} or PfPX2^{endo} as bait identified the other protein as prey (Fig. 8c). This interaction was validated with and without dithiobis(succinimidyl propionate) (DSP)-mediated crosslinking, thus supporting the idea that PfPX2 is an alveolate-specific PIP-binding effector of PfRab5a. In parallel, because inactivation of PF3D7_0929700 caused a strong growth defect (Fig. 8b), we investigated whether the conditional inactivation of this protein affects rhoptry biogenesis. SoRa spinning disk confocal microscopy revealed that early, but not late, inactivation of PF3D7_0929700 negatively impacted morphology of the rhoptry marker PfARO-mCh (Fig. 8d). These KS parasites exhibited smaller PfARO-mCh-labelled rhoptry bulbs when compared to control parasites, suggesting that PF3D7_0929700 is required during the initial stages of rhoptry biogenesis rather than for subsequent maturation. This smaller rhoptry bulbs resemble that observed in PfRab5a-KS (Supplementary Fig. 3b) and PfVPS9-KS (Fig. 7e). Together, these findings suggest several candidate PfRab5a effectors and implicate PF3D7_0929700 as a previously unrecognized regulator of rhoptry biogenesis.

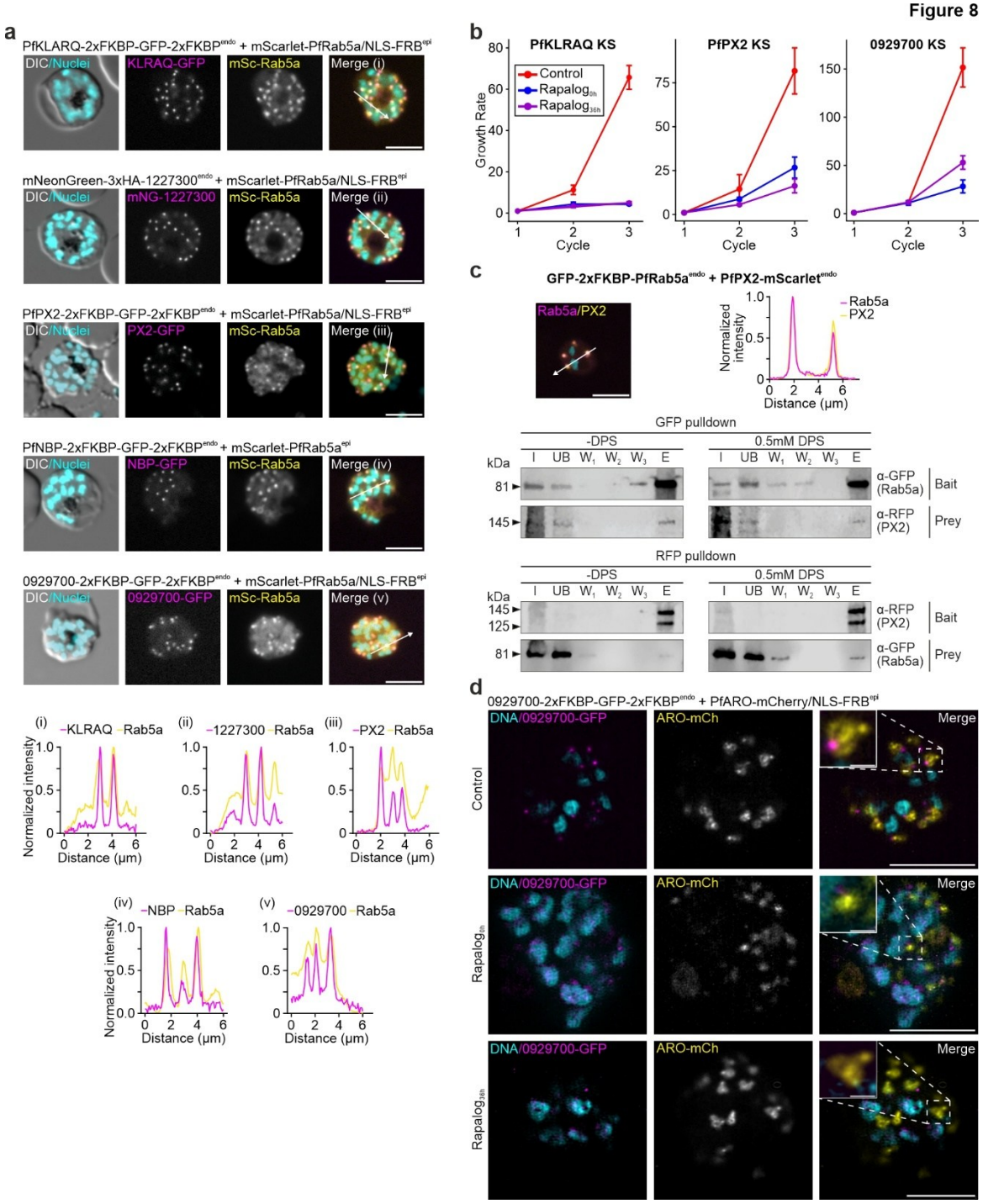


Figure 8. Novel candidates associated to PfRab5a compartments. a, Live-cell microscopy of PfKLRAQ-, PfPX2-, PfNBP- and 0929700-2xFKBP-GFP-2xFKBP^{endo} or mNeonGreen-3xHA-1227300^{endo} schizonts episomally co-expressing mSc-PfRab5a. Normalized intensity plots of these candidates and mSc-PfRab5a (i-v). **b,** Growth curve of control and KS (Rapalog$_{0h}$ and Rapalog$_{36h}$) PfKLRAQ^{endo}, PfPX2^{endo} and 0929700^{endo} parasites episomally expressing the nuclear mislocalizer (NLS-FRB-mCherry). Growth rate was normalized for initial parasitemia and measured over three cycles by flow cytometry. **c,** Co-immunoprecipitation (Co-IP) using α-GFP and α-RFP Trap beads (GFP and RFP pulldown). Experiments were performed using lysates from control GFP-2xFKBP-PfRab5a^{endo}+PfPX2-mScarlet^{endo} schizonts or incubated with 0.5 mM dithiobis(succinimidyl propionate) (DSP) for 30 minutes before lysing. A representative example of live-cell fluorescence microscopy of PfRab5a^{endo}+PfPX2^{endo} parasite and its normalized fluorescence intensity plot. Different samples were taken during the

556 procedure: I, input sample; UB, unbound; W_1-W_3, washes; E, elute. **d,** SoRa spinning disk
557 confocal microscopy of control and KS ($Rapalog_{0h}$ and $Rapalog_{36h}$) 0929700^{endo} schizonts co-
558 expressing PfARO-mCh and imaged at 48-52 hpi. Compound 2 (C2) was added to prevent
559 egress. Boxed areas were enlarged. SoRa, Super-resolution by optical re-assignment. DIC,
560 Differential interference contrast; Nuclei, Hoechst 33342; Merge, overlay of magenta, yellow
561 and cyan channels. Scale bars, 1 μm in (**d**, enlargements) and 5 μm in (**a**, **c, d**, whole cell).

Discussion

The small GTPase Rab5 is a canonical regulator of early endocytic pathways in eukaryotes. However, in *P. falciparum*, PfRab5a is dispensable for endocytosis despite being essential for parasite development[18,19]. In this study, we characterized PfRab5a as a central regulator of rhoptry and microneme biogenesis in *P. falciparum.* The apicomplexan parasites have repurposed the role of this small GTPase and other classical endocytic factors to sustain the formation of apical secretory organelles[13,18,19]. We show that PfRab5a localizes to a discrete post-Golgi compartment that is distinct from both Golgi and PfRab7 compartments[25]. The lack of colocalization with well-established markers, together with its resistance to BFA, supports its location in an uncharacterized compartment, which we have termed the PfRab5a compartment. This compartment appears to be involved in the same trafficking pathways to those described for the ELCs in *T. gondii*, which is indispensable for biogenesis of apical organelles[14,55]. Intriguingly, the ELC harbors both TgRab5a and TgRab7, in contrast to *P. falciparum*, where these GTPases occupy distinct populations or subdomains within the same compartment (Fig. 1e). Furthermore, the detection of PfRab5c in the PfRab5a proxiome suggests that both *P. falciparum* Rab5 paralogs may cooperate with each other in the same compartment, in a manner analogous to the colocalization and apical organelle trafficking-related functions of both *T. gondii* Rab5 orthologs in the ELC[13]. Although the molecular identity of this organelle remains to be fully resolved, our findings suggest that the PfRab5a has adopted a specialized function during schizont maturation or merozoite construction in *P. falciparum*, linking a canonical endocytic regulator to the biogenesis of parasite-specific secretory organelles.

Conditional inactivation of PfRab5a resulted in a severe growth defect and markedly impaired merozoite invasion. These phenotypes were associated with mistargeting and defective proteolytic processing of microneme and rhoptry proteins, indicating that proper trafficking is required for protein maturation and function. Moreover, this defect extended beyond protein sorting, negatively impacting the maturation of these apical secretory organelles themselves. Collectively, these results demonstrate that PfRab5a plays a pivotal role in the biogenesis and cargo trafficking of micronemes and rhoptries, but not basic merozoite formation or IMC development.

The proxiome of PfRab5a provided insight into the composition of this compartment, identifying proteins such as the CORVET complex and PfVPS9, consistent with an endosomal identity. Interestingly, comparison with the PfAP-1[17] and PfClathrin[56] proxiomes revealed extensive overlap in trafficking factors despite the absence of reciprocal enrichment of the bait proteins themselves. This suggests that PfRab5a compartments function downstream of the trans-Golgi sorting platform. The PfRab5a proxiome identified SNARE proteins (such as PfSYN2, PfSYN6 and PfSYN11) and PfSortilin, which potentially intersect at the PfRab5a compartment. The mistargeting of PfSortilin following PfRab5a loss suggests that PfRab5a promotes the recruitment of tethering and fusion machinery required for cargo delivery from the trans-Golgi. Thus, the presence of PfSortilin supports its established role as a major cargo receptor at the trans-Golgi, essential for apical organelle biogenesis in both *T. gondii* and *P. falciparum*[15,39,57].

In eukaryotic models, Rab5 recruits the CORVET complex, which, in conjunction with SNAREs, mediates vesicle tethering and membrane fusion with the target membrane[2]. In *P. falciparum*, the PfRab5a proxiome identified all HOPS/CORVET core subunits, and the CORVET-specific subunits PfVPS3 and PfVPS8, but not putative HOPS-specific subunits[16,17,41]. Despite PfVPS8 being annotated as transmembrane protein in PlasmoDB[58], subsequent analysis by DeepTMHMM[59] showed that it lacks predicted transmembrane domains. Structural alignments revealed clear conservation of VPS8-associated structural features[44], despite its high sequence divergence and abundance of disordered regions. The expression pattern of this elusive CORVET subunit, in conjunction with its localization in PfRab5a compartments – similar to that of invasion-specific subunit PfVPS16[41] – suggests that PfRab5a may cooperate with the CORVET complex in an invasion-related pathway in the parasite. In addition, the PfRab5a proxiome also identified the BEACH domain-containing protein (PfBDCP, PF3D7_1124100), which was recently identified in the PfVPS16 pulldown of *P. falciparum*[41] and was previously associated with the HOPS/CORVET complex and rhoptry biogenesis in *T. gondii*[60]. The presence of PfBDCP may represent a divergence from the conventional HOPS and CORVET models as reported for mini-CORVET in *Drosophila*[61], hybrid complexes[62] and unconventional complexes in human cells under stress conditions[6].

The PfRab5a proxiome also identified key regulators of the GTPase cycle, including PfVPS9, PfTBCK and PfGDI, all of which localized in PfRab5a compartments. The loss of PfVPS9 phenocopied the stage-dependent inactivation of PfRab5a, leading to defective invasion caused by defects in apical organelle biogenesis. PfVPS9 loss also altered the steady-state localization of PfRab5a, supporting its role as the GEF of PfRab5a. Our findings are consistent with those described for TgVPS9, which is required for apical organelle biogenesis and to activate TgRab5a[63].

Rab effectors are quite diverse, being associated with multiple cellular processes beyond vesicle trafficking[64]. In addition to potential regulators of PfRab5a, several effector candidates were identified in the PfRab5a proxiome. Since the endolysosomal system in *Plasmodium* is divergent, it is plausible that unique effectors have evolved to support novel trafficking pathways, including the formation of apical organelles. In this work we present five proteins of unknown function or with limited domain annotation that colocalized with PfRab5a. Of these, PfKLRAQ, PfPX2 and PF3D7_0929700 were identified as being important for parasite proliferation and linked to PfRab5a. The candidate KLRAQ domain-containing protein, the second most enriched protein in the PfRab5a proxiome, contains coiled-coil regions, raising the possibility that it functions in vesicle tethering or membrane organization, or mediates interaction with other proteins. The KLRAQ domain is present in several eukaryotic proteins, including the human protein phosphatase 1 regulatory subunit 21 (PPP1R21)[65]. Mutations in the PPP1R21 gene have been associated with disruption of endocytic sorting and endosomal trafficking[65], a process regulated by Rab5 in humans. PX2 is a conserved alveolate PIP-binding protein with an unconventional PX domain that was reported to preferentially binds to PI_3P, PI_5P and $PI_{(3,5)}P_2$[53]. In addition, pulldown experiments demonstrated that PfPX2 and PfRab5a are either

directly interacting or that PfPX2 is part of a novel complex that interacts with PfRab5a. Finally, the unknown protein PF3D7_0929700 is characterized in this study as a novel essential protein for rhoptry biogenesis. The mechanism behind this phenotype is still unclear, as PF3D7_0929700 only possesses the structural fold NAD(P)-binding Rossmann-like domain, one of the most abundant protein folds in nature, found in one-fifth of all proteins and representing a diverse array of enzymatic functions[66].

In summary, our findings establish PfRab5a as a central regulator of a previously uncharacterized secretory trafficking pathway required for apical secretory organelle biogenesis in *P. falciparum*. Our finding highlight that *P. falciparum* Rab5a-dependent trafficking has been rewired within a highly divergent endolysosomal system, such that it no longer acts as a canonical regulator of early endocytosis and instead governs parasite-specific secretory organelle biogenesis. The identification of unconventional, yet conserved *P. falciparum* Rab5a-associated factors and protein interacting partners, provides a framework for dissecting the molecular organization needed for the biogenesis of apical organelles that are essential for entry of the disease-causing parasite into the host RBC. Identification of this novel Rab5a biology offers new opportunities to exploit trafficking adaptation as potential vulnerabilities for therapeutic intervention.

Methods

SLI and CRISPR plasmid constructs

In order to generate parasite lines endogenously expressing the protein of interest (POI) fused to the C-terminal 2xFKBP-GFP-2xFKBP tag using the SLI system[19], the last ~1000 bp of the genes of PfNBP (PF3D7_0202600), PfKLRAQ (PF3D7_0406700), PfPX2 (PF3D7_0704400), PF3D7_0929700 and PfGDI (PF3D7_1038100) were amplified from gDNA as homology regions (HRs) and cloned into the SLI plasmid[19]. A variant of this SLI plasmid that endogenously co-expresses the nuclear mislocalizer was used to insert the HR of PfVPS9 (PF3D7_0815800), which was amplified from gDNA and cloned into the SLI/NLS plasmid. Another variant of the SLI plasmid based on the glmS ribozyme system[67] was used for PfTBCK (PF3D7_0724000) by fusing the 3xHA-mNeonGreen_NeoR-glmS (active ribozyme) tag in its C-terminus (plasmids were kindly provided by Arne Adler). Furthermore, double integrant parasites were generated by inserting the HR of PfPX2 into the SLI2 plasmid[54] to endogenously co-express PfPX2-mScarlet^{endo} in GFP-2xFKBP-PfRab5a^{endo} parasites. In all the variant of SLI plasmids, the HRs of the gene of interest (GOI) were inserted into the plasmids using T4 ligation or Gibson assembly[68] after digestion with NotI and AvrII (NEB). Correct integration into the parasite genome after SLI was confirmed by PCR (Supplementary Fig. 1c)[19].

The CRISPR/Cas9-mediated editing system was utilized for PfVPS8 (PF3D7_0721000), PF3D7_1227300 and PfVP2 (PF3D7_1235200). Specific guide oligonucleotides for each gene were annealed and cloned into the pDC2-Cas9-U6-hDHFRyFCU plasmid[69]. Repair templates contained two HRs of ~400 bp (5' and 3') for each gene, the fluorescence tag and a recodonized sequence of the replaced gene area. For PfVPS8 and PF3D7_1227300, a mNeonGreen-3xHA tag was introduced in their N-terminus. To generate the dimerizable Cre recombinase (DiCre)-mediated cKO PfVP2 line, two loxP sites were introduced in its ORF, with the first one located within an artificial intron close to the start of the VP2 ORF, and the second one positioned between the mCherry tag and the second HR, thus enabling the DiCre-mediated excision in DiCre-expressing B11 parasites. Correct integration into the parasite genome in these CRISPR-Cas9 lines were confirmed by PCR (Supplementary Fig. 1e,g)[52].

For localization studies of specific markers in KS parasites, a set of episomally expressed (epi) mislocalizer plasmids containing the markers PfGRASP[23], PfRab6[24], PfSortilin[15], PfRab7[25], PfAMA1[70], PfARO[33], PfRON12[34,35] and PfIMC1c[71] were utilized as previously described[17,72]. Furthermore, the sequence encoding the recodonized PfRab5a[19] was amplified and inserted into the *crt*_mScarlet-PfRab6_*nmd3*_NLS-FRB-T2A-yDHODH plasmid[17] by replacing the PfRab6 sequence. Similarly, the sequences encoding the SNARE proteins Pfv-SNARE (PF3D7_0314100), PfSYN6 (PF3D7_0530100), PfSYN2 (PF3D7_1210100), PfSYN11 (PF3D7_ 1432000) and PfGOSR1 (PF3D7_ 1469100) were amplified and cloned into the *hsp86*_mScarlet-PfRab5a-yDHODH plasmid by replacing PfRab5a.

Parasite culture, transfection and synchronization

P. falciparum 3D7 and DiCre-expressing B11 parasites[73] were maintained in RPMI medium (Gibco) containing 0.5% Albumax (Gibco), 200 mM hypoxanthine and 1-5% fresh human RBCs (B+; provided Universitätklinikum Eppendorf, Hamburg). Cultures were kept at 37°C in an appropriate atmosphere of 1% O_2, 5% CO_2 and 94% N_2 as previously described[74].

For transfection of episomal and SLI plasmids, 3D7 schizonts were purified using 60% Percoll[75] and transfected with 50 µg of plasmid DNA using an Amaxa Nucleofector II (Program U-033, Lonza)[76]. The selection of transfected parasites was carried out using either 4 nM WR99210 (Jacobus Pharmaceuticals), 2.5 µg/ml Blasticidin S (BSD, Life Technologies), or 0.9 µM DSM1 (Sigma Aldrich), depending on the construct's resistance marker. To select integrant parasites, SLI was induced by adding 400 µg/ml G418 (Sigma-Aldrich) or 0.9 µM DSM1, as previously described[19]. For CRISPR/Cas9-based gene editing, B11 parasites were isolated and electroporated simultaneously with 20 µg of pDC2-Cas9-U6-hDHFRyFCU plasmid with the desired guide sequence and 50 µg of the repair template. After selection with 4 nM WR99210 for 3 days, parasites were cultured until day 7 and plaque assays was then performed to isolate single clones. After selection, the correct integration of SLI and CRISPR constructs was confirmed by PCR and fluorescence microscopy.

To generate highly synchronous ring cultures, segmented schizonts were isolated using 60% Percoll and incubated in fresh RBCs for 4 hours at 37°C, shaking in the first 30 min. Cultures were then treated with 5% sorbitol[77] to eliminate the remaining late stages, leaving only 0-4 hpi rings for subsequent experimental procedures.

Induction of knock sideways (KS), and conditional knockdown (cKD) and knockout (cKO)

For KS induction at specific-stage parasites, 4-hour synchronized parasite cultures were split in two dishes, with one receiving 250 nM rapalog (Clontech) and the other serving as a control (without rapalog). The conditional inactivation of KS was induced in 0-4-hour rings ($Rapalog_{0h}$) and 36-40-hour schizonts ($Rapalog_{36h}$). The mislocalization of target proteins and organellar markers were examined at different time points using fluorescence microscopy.

To induce cKD in PfTBCK-glmS and parasites, 0-4-hour ring cultures were split in two dishes, with one being treated with 2.5 mM GlcN and the second one as control. The repression of protein expression was verified every 48 hours by fluorescence microscopy. To induce KO in the cKO PfVP2-mCh line, synchronized parasite culture was split in two dishes, one receiving 20 nM rapalog to induce gene excision and the other dish kept as a control (DMSO). Proper gene excision was confirmed by PCR and fluorescence microscopy.

Growth curves and invasion/egress assay

To assess parasite proliferation, parasitemia was measured by flow cytometry, with 100,000 events being counted. Staining was performed in 20 µL of 0-4hour ring cultures in 80 µL of RPMI containing 25 µg/mL SYBR Green (Sigma-Aldrich) for 40

minutes at 37°C (ring-stage staining) and measured in an ACEA NovoCyte flow cytometer. Culture was then adjusted to 0.1% parasitemia at 1% hematocrit and distributed equally for each condition (control and rapalog) to start the growth curve. The next day, the parasitemia was measured by staining 20 µL of cell suspension with 80 µL RPMI containing 4.5 µg/ml dihydroethidium (DHE, Cayman Chemical) and 5 µg/mL SYBR Green (Sigma-Aldrich) for 20 minutes at 37°C (late-stage staining). Parasitemia was measured in trophozoites for three cycles: 24-28 hpi (Cycle 1); 72-76 hpi (Cycle 2); 120-124 hpi (Cycle 3).

Parasite egress and invasion assays were assessed as previously described[16]. Briefly, 36-40 hpi schizont cultures were incubated with 1 µM C2[28] to prevent parasite egress. Immediately, culture was split in two dishes, with one dish receiving 250 nM rapalog ($Rapalog_{36h}$) and the other was kept as a control. After 8 hours, 44-48 hpi schizonts were isolated by 60% Percoll and resuspended in C2-free RPMI with fresh RBCs and the parasitemia was assessed by gating on late-stage fluorescent parasites. Cultures were then allowed to invade new RBCs after 4 hours and the parasitemia was measured again. Simultaneously, culture was synchronized with 5% sorbitol to obtain rings resulting from recent invasion events and parasitemia was measured using ring-stage staining. The egress rate and the rings per ruptured schizont were calculated as indicated:

$$\text{egress rate} = \frac{\text{Schizont parasitemia (post percoll)} - \text{Schizont parasitemia (pre sorbitol)}}{\text{Schizont parasitemia (post percoll)}} \times 100$$

$$\text{rings per ruptured schizont} = \frac{\text{Ring parasitemia (post sorbitol)}}{\text{Schizont parasitemia (post percoll)} - \text{Schizont parasitemia (pre sorbitol)}}$$

Stage Quantification

Images of Giemsa smears were acquired using a Leica microscope equipped with the immersion oil objective 100x (NA 1.25) and a Leica DMC2900 camera (Leica Microsystems), and collected using the LAS software (version V4.12.0, Leica Microsystems). Parasitemia was determined using the automated 'Parasitemia' software (https://www.gburri.org/parasitemia) by counting at least 700 RBCs per condition per replicate from the acquired images. Parasites were then counted for stage quantification and categorized as rings, trophozoites, early schizonts, late schizonts, segmenters and aberrants (parasites exhibiting large vacuolar structures or abnormal morphology).

Live-cell fluorescence and spinning disk confocal microscopy

Parasites cultures were incubated with 1 µg/mL Hoechst 33342 (Thermo Fisher) for 10 minutes at 37°C. Live-cell fluorescence images were acquired using a Leica DM6B fluorescence microscope equipped with a set of filters (DAP, L5, TXR), Leica DFC9000 GT or K8 Scientific CMOS cameras, and a Leica Plan Apochromat 100x oil objective (NA 1.4). Images were collected using the Leica Application Suite X (LAS X) software (version 3.9.1.28433, Leica Microsystems).

Super-resolution fluorescence images were acquired using a Nikon Ti2 confocal microscope equipped with a Yokogawa CSU-W1 spinning disk unit, a standard laser set (405, 488, 561 and 638nm) with emission filters (447/60, 525/30, 600/52 and 705/75), the SoRa module[78] and a Hamamatsu Orca Fusion BT camera. The 100× oil (NA 1.49) and 60× water (NA 1.27) immersion objectives were used to image live cells and expanded samples, respectively. Images were processed utilizing the functions available in the NIS Elements software (v5.42.03, Nikon). Initially, images were deconvoluted using the 3D deconvolution function, and subsequently denoised using AI. Files were exported in the .nd2 format for subsequent analysis.

Ultrastructure expansion microscopy (U-ExM)

U-ExM was performed as described[16,22]. C2-arrested control or rapalog schizont (44-48 hpi) cultures were placed in a 12-well plate containing 1 mg/mL poly-D-lysine-coated 12 mm round coverslips (Thermo-Fisher) and incubated for 30 minutes at 37°C. After settling, excess culture was removed and adhered cells were fixed with 4% paraformaldehyde and 0.1% glutaraldehyde in PBS for 30 minutes at 37°C. Coverslips were then washed twice with PBS and incubated overnight at 37°C with 1 mL of anchoring solution (0.7% formaldehyde and 1% acrylamide in PBS). Coverslips were then removed from the anchoring solution, dipped in PBS and allowed to dry briefly.

For gel polymerization, 35 µL of monomer solution (19% sodium acrylate (Sigma), 10% acrylamide (Sigma) and 0.1% N,N'-methylenebisacrylamide (Sigma) in PBS) was pipetted onto a parafilm on a humid chamber on ice, followed by addition of 5 µL of 10% tetraethylenediamine (TEMED, ThermoFisher) and 5 µL of 10% ammonium persulfate (APS, ThermoFisher). Each drop was rapidly covered with the coverslip, with the cell side facing down, and kept for 5 minutes on an iced container to allow gel penetration, followed by incubation for 1 hour at 37°C for full gel polymerization. Samples were then transferred to a new container with denaturing solution (200 mM sodium dodecyl sulphate (SDS), 200 mM NaCl, 50 mM Tris at pH 9) and incubated for 15 minutes at RT to detach the coverslip from the cell-embedded gel. The gels were then incubated in fresh denaturing solution at 95°C for 90 minutes.

After denaturation, gels were transferred to a larger container and covered with ddH_2O for 30 minutes, followed overnight incubation with fresh ddH_2O to allow full gel expansion. Gels were cut into small pieces for staining. Pieces were shrunk by two rounds of 15-minutes incubations in PBS. For antibody staining, gels were incubated in blocking solution (3% BSA in PBS) for 1hour at RT, followed by incubation with 1:500 of mouse α-RAP1 primary antibody (European Malaria Reagent Repository) in 1% BSA in PBS with 0.1% Triton-X100 (PBST) for 2.5 hours at 37°C. After three washes with PBST, gels were incubated with 1:1000 of α-mouse conjugated with Alexa-Fluor 488 (AF-488) in 1% BSA in PBST. After three washes with PBST, the gels were stained with 10 µg/mL NHS-ester conjugated to either AF-594 or AF-647 (ThermoFisher) in PBS for 2.5 hours RT, protected from light. Gels were then transferred to larger container with ddH_2O for a second round of expansion for 30minutes, then kept overnight on fresh ddH_2O with 4 µg/mL Hoechst 33342 (Thermo Fisher). After final

ddH$_2$O washing step, gels were prepared for imaging by placing it in a 35 mm imaging dish (Ibidi, Cat No. 81156) coated with poly-D-lysine.

Western Blot

Schizonts were isolated using 80% Percoll, washed and then lysed with 4% SDS, 0.5% Triton X-100, and 0.5X PBS containing cOmplete™ Protease Inhibitor Cocktail (PIC, Roche). Lysates were centrifuged at maximum speed for 20 minutes at 4°C. Subsequently, supernatants were resuspended in 5X SDS sample buffer and boiled at 95°C for 5 minutes. Proteins were separated using 10% polyacrylamide or 4–12% precast (BioRad) gels and transferred to MetOH-activated PVDF membranes using a tank blot device (Bio-Rad). After transfer, membranes were air-dried, reactivated and blocked with 5% milk in TBS for 2 hours at RT. Primary antibodies were diluted in 2.5% milk in TBS containing 0.01% Tween 20 (TBST) and incubated overnight at 4°C: mouse α-GFP (1:1,000, Invitrogen), rabbit α-RFP (1:1000, ab167453, Abcam), α-RAP1[79] (1:5,000, European Malaria Reagent Repository), and rabbit α-BiP[23] (1:2000). After three washes with TBST, the membranes were incubated with IRDye 800CW/700CW goat α-mouse or α-rabbit (1:10,000, LICORbio) secondary antibody in 2.5% milk in TBST for 2 hours at RT. Fluorescent signals were visualized using Odyssey Fc Imager (version 5.2.5, LICOR Biosciences). Intensity of band signals was measured using the image analysis software FIJI (ImageJ, version 1.54s)[80].

Brefeldin A (BFA) assay

Brefeldin A (BFA) treatment was performed as previously described[25]. Parasite cultures were synchronized with 5% D-Sorbitol to obtain 0-18-hpi rings, then split into two dishes. At 24-42 hpi, 5 µg/mL of BFA was added to one culture and the same volume of DMSO to another culture. Upon 1- and 2-hour incubation, parasites were collected, stained with 1µg/µL Hoechst 33342 and imaged. The number of GFP foci was manually counted, with only single infections (one parasite per RBC) being measured.

Rhoptry and microneme secretion Assay

The secretion assay was adapted according to previously described protocols[81]. Parasites were synchronized to a 4-hour window at 10-15% parasitemia. Following a 36-hour period, 36-40 hpi schizont cultures were split in two dishes, with one kept as a control, while the other received 250 nM rapalog. After 4 hours (40-44 hpi), C2 was added to cultures to allow schizonts to complete maturation without egressing. At 48-52 hpi, cultures were split again, in one half the mature schizonts were isolated using 80% Percoll, and processed for western blot as described above. The other half was kept in culture, washing out the C2 and replacing it with 50 µM E64 to allow parasite egress while simultaneously inhibiting RBC membrane rupture. Parasites were then incubated for 30 minutes to allow merozoite egress and secretion of apical organelle contents into the unruptured RBCs. Subsequently, post-egress (+E64) parasites were isolated using 80% Percoll and processed for western blot analysis.

Dimerization inducible quantitative proximity dependent biotinylation identification (DIQ-BioID)

To perform DIQ-BioID[38], the biotin ligase miniTurbo fused to the FRB-mCherry tag (miniTurbo-FRB-mCherry) was episomally expressed in GFP-2xFKBP-Rab5a^{endo} parasites. Upon rapalog addition, miniTurbo is recruited to PfRab5a foci through FKBP–FRB dimerization, enabling biotinylation of PfRab5a-associated proteins and compartment neighbors. A tightly synchronized 150 mL culture at 10-15% parasitemia and 5% hematocrit containing late schizonts (36-40 hours) was isolated using 80% Percoll. Schizonts were then washed twice, split into two cultures, one without rapalog (control) and another with 250 nM rapalog (rapalog), both cultures incubated for 50 minutes at 37°C. After this first 20 minutes, both control and rapalog-treated cultures were incubated with 50 µM biotin (Sigma-Aldrich) for 30 minutes at 37°C. Parasites were pelleted, washed with PBS and lysed in the lysis buffer (50 mM Tris-HCl pH 7.5, 500 mM NaCl, 1 mM DTT, 1 mM PMSF, 2× PIC, and 1% Triton-X-100) and frozen at −80°C until its use. Complete lysis of the cells was achieved by three consecutive freeze-thaw cycles, lysates were then centrifuged to a maximum speed for 30 minutes at 4°C. Supernatant was collected and stored at −80°C.

For purification of biotinylated proteins, 50 µL of streptavidin Sepharose beads (GE Healthcare) was added to the supernatants and incubated overnight with over-head rotation at 4°C. Beads were washed twice with lysis buffer, twice with Tris-HCl (pH 8.5) and twice with 100 mM triethylammonium bicarbonate buffer (TEAB) pH 7.5 (Sigma-Aldrich). To perform on-bead-digestion, beads were resuspended in 200 µL of 100 nM TEAB pH 7.5 and incubated with 1 µg trypsin (Roche) at 37°C overnight while shaking. An additional 0.5 µg of trypsin was added the next day and incubated under the same conditions for 2 hours to ensure complete digestion. Bead and peptide mix were placed onto a spin column (Pierce Spin Columns with snap cap, Thermo Scientific) placed in a low binding tube (Low Protein Binding Microcentrifuge tubes, Thermo Scientific) and centrifuged at 600 g at 4°C for 5 minutes. Three additional elution steps were performed, twice with 150 µL TEAB and the final one with HPLC grade water. Samples were then dried using a SpeedVac (Thermo Fisher Scientific) and stored at −20°C.

Dried samples were sent to the Proteomics Core Facility at EMBL Heidelberg and processed as previously described[32]. Peptides were in 1% Formic acid/ 4% acetonitrile, sonicated in the ultrasonic bath for 5 minutes and desalted using an OASIS® HLB µElution Plate (Waters). Peptide sample labelling was then performed in 50 mM HEPES pH8.5 and labelled with TMT6plex Isobaric Label Reagent (ThermoFisher). Subsequently, samples were pooled and purified from unreacted TMT label using OASIS® HLB µElution Plate (Waters).

An UltiMate 3000 RSLC nano LC system (Dionex) fitted with a trapping cartridge (µ-Precolumn C18 PepMap 100, 5 µm, 300 µm i.d. x 5 mm, 100 Å) and an analytical column (nanoEase™ M/Z HSS T3 column 75 µm x 250 mm C18, 1.8 µm, 100 Å, Waters). Trapping was carried out with a constant flow of solvent A (0.1% formic acid in water) at 30 µL/min onto the trapping column for 6 minutes. Subsequently, peptides were eluted via the analytical column with a constant flow of 0.3 µL/min with increasing

percentage of solvent B (0.1% formic acid in acetonitrile) from 2% to 4% in 4 minutes, from 4% to 8% in 2 minutes, then 8% to 28% for a further 37 minutes, and finally from 28% to 40% in another 9 minutes. The outlet of the analytical column was coupled directly to a QExactive plus (Thermo) mass spectrometer using the proxeon nanoflow source in positive ion mode. Peptides were introduced into the QExactive plus via a Pico-Tip Emitter 360 µm OD x 20 µm ID; 10 µm tip (New Objective) and an applied spray voltage of 2.1 kV. The capillary temperature was set at 275°C. Full mass scan was acquired with mass range 375-1200 m/z in profile mode with resolution of 70000. The filling time was set at maximum of 10 ms with a limitation of $3x10^6$ ions. Data dependent acquisition (DDA) was performed with the resolution of the Orbitrap set to 17500, with a fill time of 50 ms and a limitation of $2x10^5$ ions. A normalized collision energy of 32 was applied. Dynamic exclusion time of 30 seconds was used. The peptide match algorithm was set to 'preferred' and charge exclusion 'unassigned', charge states 1, 5 - 8 were excluded. MS2 data was acquired in profile mode.

IsobarQuant and Mascot (v2.2.07) were used to process the acquired data, which was searched against a Uniprot *Plasmodium falciparum* (UP000001450) proteome database containing common contaminants and reversed sequences. The following modifications were included into the search parameters: Carbamidomethyl (C) and TMT10 (K) (fixed modification), Acetyl (Protein N-term), Oxidation (M) and TMT10 (N-term) (variable modifications). For the full scan (MS1) a mass error tolerance of 10 ppm and for MS/MS (MS2) spectra of 0.02 Da was set. Further parameters were set: Trypsin as protease with an allowance of maximum two missed cleavages: a minimum peptide length of seven amino acids; at least two unique peptides were required for a protein identification. The false discovery rate (FDR) on peptide and protein level was set to 0.01.

Gene ontology (GO) enrichment analysis

GO term analysis was performed by searching the biological process GO terms and enrichment with PlasmodDB[58] for the candidates found the PfRab5a BioID. In order to reduce redundancy in the GO terms obtained, the terms with adjusted p-value (<0.05 using the Benjamini-Hochberg method) were analyzed in the REVIGO platform[82]. This produced a reduced GO term list with average p-value.

Protein structure prediction

Predicted proteins were obtained from the AlphaFold protein structure database (https://alphafold.ebi.ac.uk/). For PfVPS8 (PF3D7_0721000), there was no available structure prediction, so the whole protein structure was predicted using the AlphaFold3 on the server[43]. Predicted template modelling (pTM) scores were taken from the AlphaFold3 predictions.

For structure alignment search, the whole sequence of the protein was submitted to the FoldSeek server[45] (https://search.foldseek.com/) in the AlphaFold/Uniprot50_v6, AlphaFold/Swiss-Prot_v6, AlphaFold/Proteome_v6 and PDB100_20240101 databases, the 3Di/AA mode was used with no iterations. The highest scoring structural homologs (highest sequence identity and E-value) were considered for

structural comparison. For structural alignment of PfVPS8, the modelled PF3D7_0721000 β-propeller (498-1071 aa) was aligned with the N-terminal β-propeller of mouse (UniProt: Q0P5W1 95-515aa), human (UniProt: Q8N3P4 95-513 aa) and yeast (UniProt: O13756 93-513 aa) VPS8. The resulting FoldSeek structure alignment was taken and processed for visualization in ChimeraX (UC San Francisco, v1.11.1).

The multimer structure prediction of PfVPS9-PfRab5a was performed using AlphaFold3[43]. Scores for pTM and interface predicted template modelling (ipTM) were taken from AlphaFold3. Structures were visualized in ChimeraX.

Co-immunoprecipitation assay (Co-IP)

Synchronous cultures with >7–10% parasitemia were enriched for late stages using 80% Percoll. Parasite pellets were split for processing with or without crosslinking. For crosslinking, pellets were treated with 0.5 mM dithio-bis(succinimidyl propionate) (DSP, Sigma-Aldrich) for 30 minutes at RT, quenched with 25 mM Tris-HCl and washed with PBS. Samples were subsequently divided for α-GFP or α-RFP pulldown assays.

Samples were lysed in RIPA lysis buffer (10 mM Tris-HCl pH 7.5, 150 mM NaCl, and 1% Triton X-100) containing 1 mM DTT, 1 mM PMSF and 2× protease inhibitor cocktail tablets (Roche). Lysates were then subjected to three freeze–thaw cycles and clarified by centrifugation (16,000 g, 30 minutes, 4 °C). The supernatant was adjusted to 1 ml with RIPA base buffer (10 mM Tris-HCl pH 7.5, 150 mM NaCl) containing protease inhibitors, and an aliquot was collected as input fraction.

For immunoprecipitation, lysates were incubated with GFP- or RFP-Trap agarose beads (Chromotek) overnight at 4 °C with rotation. Beads were collected by centrifugation (500 g for 5minutes at 4 °C) and the supernatant was retained as the unbound fraction. Beads were washed three times with RIPA base buffer containing protease inhibitors (500 g, 5minutes, 4 °C). Bound proteins were eluted in 4% SDS, 0.5% Triton X-100 and 0.5× PBS at 95 °C for 5 minutes. Subsequently, the input, unbound, wash and eluate fractions were analysed by western blot.

Data analysis

Statistical analysis and graphics were performed using R (v ImageJ 4.5.2) with the latest version of the packages *tidyverse*, *rstatix*, and *ggpubr*. Heatmap of PfRab5 proxiome showing the HOPS/CORVET subunits was performed using GraphPad Prism version 8 (GraphPad Software). All experimental replicates represent independent culture vessels. Statistical significance, when calculated, is from at least two independent experiments, p-value bellow 0.05 was considered significant. FIJI[80] (v1.54p) was used for microscopy image processing, intensity line profile and signal intensity measurement.

For measuring the distance from between PfRab5a, PfRab6, and PRab7 compartments in SoRa spinning disk confocal microscopy images, the distance analysis plugin (DiAna, v1.54)[83] for FIJI was used. Object segmentation was done using the iterative segmentation option, then the distance from the center of the

PfRab5a objects from the center of the closest PfRab6/PfRab7 object was obtained. Distances were measured for each PfRab5a foci in the schizont imaged.

For the quantification of PfARO-mCh signal, the deconvolved images were imported into the microscopy analysis software Imaris (v9.8.2, BitPlane AG), and processed using a surface identification based on previous protocols.[84] The PfARO-mCh signal was thresholded based on signal intensity, touching objects splitting with a seed diameter of 0.4µm and then filtered using the quality parameter (>157). To quantify the rhoptry volume of U-ExM samples, a different Imaris surface identification pipeline was used from a different protocol[16]. Deconvolved images were imported and analyzed in batch mode to ensure identical processing. For rhoptry surface identification, the NHS-ester signal was thresholded based on high intensity to isolate rhoptries due to their high signal. Touching objects were split with a seed diameter of 0.4 µm, then all identified objects were further filtered based on volume (>168 voxels) to and the quality (>831) parameter provided by Imaris. For nuclei, the Hoechst signal intensity was thresholded as before and the created objects splits using a seed diameter of 3 µm. Volume measurements of single rhoptries were analyzed and plotted using R (v4.5.2).

Data Availability

The mass spectrometry proteomics data have been deposited to the ProteomeXchange Consortium via the PRIDE[85] partner repository with the dataset identifier PXD081695. PlasmoDB accession codes for all proteins studied here are shown directly in the figures and in the manuscript. Source data are provided with this paper.

Acknowledgments

We acknowledge the microscopy support from the Advanced Light and Fluorescence Microscopy (ALFM) facility at the Centre for Structural Systems Biology (CSSB). This work was supported by the Deutsche Forschungsgemeinschaft GRK2771–No 453548970 (GBF, TWG); Leibniz ScienceCampus InterACt W75/2022 InterACt and "Hamburg-X Infektionsforschung" (GBF, TWG); CSSB grant KIF 2024-9 (TWG, LZ). DWW acknowledge support of the Alexander von Humboldt Foundation. We thank Jacobus Pharmaceuticals for WR99210. We gratefully acknowledge Jennifer Schwarz and Frank Stein for the mass spectroscopy support from the Proteomic Core facility at EMBL Heidelberg. We also acknowledge Arne Adler for providing the SLI HA-mNeonGreen-glmS construct. The funders had no role in study design, data collection and analysis, decision to publish or preparation of the manuscript.

Author contributions

G.B.F., T.S. and T.G. conceptualized the project; G.B.F. designed and performed most experiments. G.B.F. and L.Z. performed the AlphaFold structure predictions. G.B.F. generated most parasite lines, with Y.G. generating one line (PfKLRAQ). T.N.P., N.P., J.P.M.R. and J.C.M. assisted in several experiments and in transfection of episomal constructs. G.B.F. and J.C.M. did the data analysis. C.L. assisted in the BioID and MS analysis. D.W.W. assisted in designing the invasion assay and reviewed the data during the project. J.M.M. assisted in CRISPR construct design and provided all

SNARE episomal plasmids. The original draft was written by G.B.F. and J.C.M., revised and edited by J.C.M. and T.G., and reviewed by all authors.

References:

1. Venkatesan, P. WHO world malaria report 2024. *Lancet Microbe* **6**, 101073 (2025).
2. Borchers, A. C., Langemeyer, L. & Ungermann, C. Who's in control? Principles of rab gtpase activation in endolysosomal membrane trafficking and beyond. *Journal of Cell Biology* **220**, (2021).
3. Füllbrunn, N., Ungermann, C. & Langemeyer, L. Endolysosomal transport at the crossroads of cellular signaling. *Trends Cell Biol.* **0**, (2026).
4. Homma, Y., Hiragi, S. & Fukuda, M. Rab family of small GTPases: an updated view on their regulation and functions. *FEBS Journal* **288**, 36–55 (2021).
5. kleine Balderhaar, H. J. & Ungermann, C. CORVET and HOPS tethering complexes – coordinators of endosome and lysosome fusion. *J. Cell Sci.* **126**, 1307–1316 (2013).
6. van der Beek, J., Jonker, C., van der Welle, R., Liv, N. & Klumperman, J. CORVET, CHEVI and HOPS – Multisubunit tethers of the endo-lysosomal system in health and disease. *J. Cell Sci.* **132**, (2019).
7. Poteryaev, D., Datta, S., Ackema, K., Zerial, M. & Spang, A. Identification of the switch in early-to-late endosome transition. *Cell* **141**, 497–508 (2010).
8. Rink, J., Ghigo, E., Kalaidzidis, Y. & Zerial, M. Rab conversion as a mechanism of progression from early to late endosomes. *Cell* **122**, 735–749 (2005).
9. Singh, M. K. *et al.* Protein delivery to vacuole requires SAND protein-dependent Rab GTPase conversion for MVB-vacuole fusion. *Curr. Biol.* **24**, 1383–1389 (2014).
10. Spielmann, T., Gras, S., Sabitzki, R. & Meissner, M. Endocytosis in Plasmodium and Toxoplasma Parasites. *Trends Parasitol.* **36**, 520–532 (2020).
11. Tomavo, S., Slomianny, C., Meissner, M. & Carruthers, V. B. Protein Trafficking through the Endosomal System Prepares Intracellular Parasites for a Home Invasion. *PLoS Pathog.* **9**, e1003629 (2013).
12. Tomavo, S. Evolutionary repurposing of endosomal systems for apical organelle biogenesis in Toxoplasma gondii. *Int. J. Parasitol.* **44**, 133–138 (2014).
13. Kremer, K. *et al.* An Overexpression Screen of Toxoplasma gondii Rab-GTPases Reveals Distinct Transport Routes to the Micronemes. *PLoS Pathog.* **9**, e1003213 (2013).
14. Sangaré, L. O. *et al.* Unconventional endosome-like compartment and retromer complex in Toxoplasma gondii govern parasite integrity and host infection. *Nat. Commun.* **7**, 11191 (2016).
15. Hallée, S., Boddey, J. A., Cowman, A. F. & Richard, D. Evidence that the Plasmodium falciparum Protein Sortilin Potentially Acts as an Escorter for the Trafficking of the Rhoptry-Associated Membrane Antigen to the Rhoptries. *mSphere* **3**, (2018).
16. Mesén-Ramírez, J. P. *et al.* HOPS/CORVET tethering complexes are critical for endocytosis and protein trafficking to invasion related organelles in malaria parasites. *PLoS Pathog.* **21**, e1013053 (2025).
17. Cubillán-Marín, J. *et al.* Vesicle adaptors in malaria parasites show conservation and flexibility of protein sorting machinery. *Journal of Cell Biology* **224**, (2025).

18. Sabitzki, R. *et al.* Role of Rabenosyn-5 and Rab5b in host cell cytosol uptake reveals conservation of endosomal transport in malaria parasites. *PLoS Biol.* **22**, e3002639 (2024).

19. Birnbaum, J. *et al.* A genetic system to study Plasmodium falciparum protein function. *Nat. Methods* **14**, 450–456 (2017).

20. Haruki, H., Nishikawa, J. & Laemmli, U. K. The anchor-away technique: rapid, conditional establishment of yeast mutant phenotypes. *Mol. Cell* **31**, 925–32 (2008).

21. Robinson, M. S., Sahlender, D. A. & Foster, S. D. Rapid inactivation of proteins by rapamycin-induced rerouting to mitochondria. *Dev. Cell* **18**, 324–31 (2010).

22. Liffner, B. *et al.* Atlas of Plasmodium falciparum intraerythrocytic development using expansion microscopy. *Elife* **12**, (2023).

23. Struck, N. S. *et al.* Re-defining the Golgi complex in *Plasmodium falciparum* using the novel Golgi marker *Pf* GRASP. *J. Cell Sci.* **118**, 5603–5613 (2005).

24. Van Wye, J. *et al.* Identification and localization of rab6, separation of rab6 from ERD2 and implications for an 'unstacked' Golgi, in Plasmodium falciparum. *Mol. Biochem. Parasitol.* **83**, 107–120 (1996).

25. Krai, P., Dalal, S. & Klemba, M. Evidence for a Golgi-to-Endosome Protein Sorting Pathway in Plasmodium falciparum. *PLoS One* **9**, e89771 (2014).

26. Lippincott-Schwartz, J., Yuan, L. C., Bonifacino, J. S. & Klausner, R. D. Rapid redistribution of Golgi proteins into the ER in cells treated with brefeldin A: Evidence for membrane cycling from Golgi to ER. *Cell* **56**, 801–813 (1989).

27. Morrissette, N. S. & Sibley, L. D. Cytoskeleton of apicomplexan parasites. *Microbiol. Mol. Biol. Rev.* **66**, 21–38 (2002).

28. Taylor, H. M. *et al.* The malaria parasite cyclic GMP-dependent protein kinase plays a central role in blood-stage schizogony. *Eukaryot. Cell* **9**, 37–45 (2010).

29. Tonkin, M. L. *et al.* Host cell invasion by apicomplexan parasites: Insights from the co-structure of AMA1 with a RON2 peptide. *Science (1979).* **333**, 463–467 (2011).

30. Salmon, B. L., Oksman, A. & Goldberg, D. E. Malaria parasite exit from the host erythrocyte: a two-step process requiring extraerythrocytic proteolysis. *Proc. Natl. Acad. Sci. U. S. A.* **98**, 271–6 (2001).

31. Liffner, B., Balbin, J. M., Wichers, J. S., Gilberger, T. W. & Wilson, D. W. The Ins and Outs of Plasmodium Rhoptries, Focusing on the Cytosolic Side. *Trends in Parasitology* vol. 37 638–650 Preprint at https://doi.org/10.1016/j.pt.2021.03.006 (2021).

32. Geiger, M. *et al.* Structural Insights Into PfARO and Characterization of its Interaction With PfAIP. *J. Mol. Biol.* **432**, 878–896 (2020).

33. Cabrera, A. *et al.* Dissection of minimal sequence requirements for rhoptry membrane targeting in the malaria parasite. *Traffic* **13**, 1335–1350 (2012).

34. Ito, D. *et al.* Antibodies against a Plasmodium falciparum RON12 inhibit merozoite invasion into erythrocytes. *Parasitol. Int.* **68**, 87–91 (2019).

35. Knuepfer, E. *et al.* RON12, a novel Plasmodium-specific rhoptry neck protein important for parasite proliferation. *Cell. Microbiol.* **16**, 657–672 (2014).

36. Ridley, R. G. *et al.* Characterisation and sequence of a protective rhoptry antigen from Plasmodium falciparum. *Mol. Biochem. Parasitol.* **41**, 125–134 (1990).

37. Howard, R. F., Narum, D. L., Blackman, M. & Thurman, J. Analysis of the processing of Plasmodium falciparum rhoptry-associated protein 1 and localization of Pr86 to schizont rhoptries and p67 to free merozoites. *Mol. Biochem. Parasitol.* **92**, 111–122 (1998).

38. Birnbaum, J. *et al.* A Kelch13-defined endocytosis pathway mediates artemisinin resistance in malaria parasites. *Science (1979).* **367**, 51–59 (2020).

39. Sloves, P. J. *et al.* Toxoplasma sortilin-like receptor regulates protein transport and is essential for apical secretory organelle biogenesis and host infection. *Cell Host Microbe* **11**, 515–527 (2012).

40. Jahn, R., Cafiso, D. C. & Tamm, L. K. Mechanisms of SNARE proteins in membrane fusion. *Nat. Rev. Mol. Cell Biol.* **25**, 101–118 (2024).

41. Lauruol, F., Galaup, T., Bourgeois, A., Sergerie, A. & Richard, D. The *Plasmodium falciparum* homolog of Vps16 interacts with the core members of the Vps-C tethering complex. *mSphere* **10**, (2025).

42. Ganesan, S. M. *et al.* Yeast dihydroorotate dehydrogenase as a new selectable marker for Plasmodium falciparum transfection. *Mol. Biochem. Parasitol.* **177**, 29–34 (2011).

43. Abramson, J. *et al.* Accurate structure prediction of biomolecular interactions with AlphaFold 3. *Nature 2024 630:8016* **630**, 493–500 (2024).

44. Shvarev, D. *et al.* Structure of the endosomal CORVET tethering complex. *Nat. Commun.* **15**, 5227 (2024).

45. van Kempen, M. *et al.* Fast and accurate protein structure search with Foldseek. *Nat. Biotechnol.* **42**, 243–246 (2024).

46. Xu, J. & Zhang, Y. How significant is a protein structure similarity with TM-score = 0.5? *Bioinformatics* **26**, 889 (2010).

47. Carney, D. S., Davies, B. A. & Horazdovsky, B. F. Vps9 domain-containing proteins: activators of Rab5 GTPases from yeast to neurons. *Trends Cell Biol.* **16**, 27–35 (2006).

48. Müller, M. P. & Goody, R. S. Molecular control of Rab activity by GEFs, GAPs and GDI. *Small GTPases* **9**, 5–21 (2018).

49. Pfeffer, S. & Aivazian, D. Targeting Rab GTPases to distinct membrane compartments. *Nature Reviews Molecular Cell Biology 2004 5:11* **5**, 886–896 (2004).

50. Albert, Š., Will, E. & Gallwitz, D. Identification of the catalytic domains and their functionally critical arginine residues of two yeast GTPase-activating proteins specific for Ypt/Rab transport GTPases. *The EMBO Journal 1999 18:19* **18**, 5216–5225 (1999).

51. Wilmes, S. & Kümmel, D. Insights into the role of the membranes in Rab GTPase regulation. *Curr. Opin. Cell Biol.* **83**, 102177 (2023).

52. Knuepfer, E., Napiorkowska, M., van Ooij, C. & Holder, A. A. Generating conditional gene knockouts in Plasmodium - a toolkit to produce stable DiCre recombinase-expressing parasite lines using CRISPR/Cas9. *Sci. Rep.* **7**, 3881 (2017).

53. Roucheray, S. *et al.* Characterization of a phosphoinositide-binding protein containing a PHOX homology domain in the malaria parasite Plasmodium falciparum. *Scientific Reports 2025 15:1* **15**, 36867 (2025).

54. Cronshagen, J. *et al.* A system for functional studies of the major virulence factor of malaria parasites. *Elife* **13**, (2025).

55. Miranda, K. *et al.* Characterization of a novel organelle in Toxoplasma gondii with similar composition and function to the plant vacuole. *Mol. Microbiol.* **76**, 1358–1375 (2010).

56. Birnbaum, J. *et al.* A Kelch13-defined endocytosis pathway mediates artemisinin resistance in malaria parasites. *Science (1979).* **367**, 51–59 (2020).

57. Hallée, S., Counihan, N. A., Matthews, K., de Koning-Ward, T. F. & Richard, D. The malaria parasite Plasmodium falciparum Sortilin is essential for merozoite formation and apical complex biogenesis. *Cell. Microbiol.* **20**, (2018).

58. Roos, D. S. *et al.* PlasmoDB: An integrative database of the Plasmodium falciparum genome. Tools for accessing and analyzing finished and unfinished sequence data. *Nucleic Acids Res.* **29**, 66 (2001).

59. Hallgren, J. *et al.* DeepTMHMM predicts alpha and beta transmembrane proteins using deep neural networks. *bioRxiv* 2022.04.08.487609 (2022) doi:10.1101/2022.04.08.487609.

60. Morlon-Guyot, J. *et al.* A proteomic analysis unravels novel CORVET and HOPS proteins involved in Toxoplasma gondii secretory organelles biogenesis. *Cell. Microbiol.* **20**, e12870 (2018).

61. Lőrincz, P. *et al.* MiniCORVET is a Vps8-containing early endosomal tether in drosophila. *Elife* **5**, (2016).

62. Terawaki, S., Vasilev, F., Moriwaki, T. & Otomo, T. HOPS, CORVET and newly-identified Hybrid tethering complexes contribute differentially towards multiple modes of endocytosis. *Sci. Rep.* **13**, 18734 (2023).

63. Sakura, T. *et al.* A Critical Role for Toxoplasma gondii Vacuolar Protein Sorting VPS9 in Secretory Organelle Biogenesis and Host Infection. *Sci. Rep.* **6**, 1–13 (2016).

64. Grosshans, B. L., Ortiz, D. & Novick, P. Rabs and their effectors: achieving specificity in membrane traffic. *Proc. Natl. Acad. Sci. U. S. A.* **103**, 11821–7 (2006).

65. Rehman, A. U. *et al.* Biallelic loss of function variants in PPP1R21 cause a neurodevelopmental syndrome with impaired endocytic function. *Hum. Mutat.* **40**, 267–280 (2019).

66. Medvedev, K. E., Kinch, L. N., Dustin Schaeffer, R., Pei, J. & Grishin, N. V. A Fifth of the Protein World: Rossmann-like Proteins as an Evolutionarily Successful Structural unit. *J. Mol. Biol.* **433**, 166788 (2021).

67. Prommana, P. *et al.* Inducible Knockdown of Plasmodium Gene Expression Using the glmS Ribozyme. *PLoS One* **8**, e73783 (2013).

68. Gibson, D. G. *et al.* Enzymatic assembly of DNA molecules up to several hundred kilobases. *Nat. Methods* **6**, 343–345 (2009).

69. Alder, A. *et al.* The role of Plasmodium V-ATPase in vacuolar physiology and antimalarial drug uptake. *Proc. Natl. Acad. Sci. U. S. A.* **120**, e2306420120 (2023).

70. Triglia, T. *et al.* Apical membrane antigen 1 plays a central role in erythrocyte invasion by Plasmodium species. *Mol. Microbiol.* **38**, 706–718 (2000).

71. Hu, G. *et al.* Transcriptional profiling of growth perturbations of the human malaria parasite Plasmodium falciparum. *Nat. Biotechnol.* **28**, 91–98 (2010).

72. Schmidt, S. *et al.* The Kelch13 compartment contains highly divergent vesicle trafficking proteins in malaria parasites. *PLoS Pathog.* **19**, e1011814 (2023).

73. Perrin, A. J. *et al.* The Actinomyosin Motor Drives Malaria Parasite Red Blood Cell Invasion but Not Egress. *mBio* **9**, (2018).

74. Trager, W. & Jensen, J. B. Continuous culture of Plasmodium falciparum: its impact on malaria research. *Int. J. Parasitol.* **27**, 989–1006 (1997).

75. RIVADENEIRA, E. M., WASSERMAN, M. & ESPINAL, C. T. Separation and Concentration of Schizonts of *Plasmodium falciparum* by Percoll Gradients1. *J. Protozool.* **30**, 367–370 (1983).

76. Moon, R. W. *et al.* Adaptation of the genetically tractable malaria pathogen Plasmodium knowlesi to continuous culture in human erythrocytes. *Proc. Natl. Acad. Sci. U. S. A.* **110**, 531–536 (2013).

77. Lambros, C. & Vanderberg, J. P. Synchronization of Plasmodium falciparum erythrocytic stages in culture. *Journal of Parasitology* **65**, (1979).

78. DuBose, T. B., LaRocca, F., Farsiu, S. & Izatt, J. A. Super-resolution retinal imaging using optically reassigned scanning laser ophthalmoscopy. *Nat. Photonics* **13**, 257–262 (2019).

79. Hall, R. *et al.* Antigens of the erythrocytic stages of the human malaria parasite Plasmodium falciparum detected by monoclonal antibodies. *Mol. Biochem. Parasitol.* **7**, 247–265 (1983).

80. Schindelin, J. *et al.* Fiji: an open-source platform for biological-image analysis. *Nature Methods 2012 9:7* **9**, 676–682 (2012).

81. Liffner, B. *et al.* PfCERLI1 is a conserved rhoptry associated protein essential for Plasmodium falciparum merozoite invasion of erythrocytes. *Nat. Commun.* **11**, 1–14 (2020).

82. Supek, F., Bošnjak, M., Škunca, N. & Šmuc, T. REVIGO Summarizes and Visualizes Long Lists of Gene Ontology Terms. *PLoS One* **6**, e21800 (2011).

83. Gilles, J. F., Dos Santos, M., Boudier, T., Bolte, S. & Heck, N. DiAna, an ImageJ tool for object-based 3D co-localization and distance analysis. *Methods* **115**, 55–64 (2017).

84. Liffner, B. *et al.* Cell biological analysis reveals an essential role for Pfcerli2 in erythrocyte invasion by malaria parasites. *Commun. Biol.* **5**, 121 (2022).

85. Perez-Riverol, Y. *et al.* The PRIDE database at 20 years: 2025 update. *Nucleic Acids Res.* **53**, D543–D553 (2025).

Supplementary Files

This is a list of supplementary files associated with this preprint. Click to download.

- SupplementaryData4.docx
- SupplementaryData5.docx
- SupplementaryData3.docx
- SupplementaryData2.docx
- FariasetalSupplementaryFiguresfinal.pdf
- SupplementaryData1.xlsx
- DescriptionofAdditionalSupplementaryandSourceDatafiles.pdf
- SourceData.zip